Measurement 255 (2025) 117966

Contents lists available at ScienceDirect

Measurement

journal homepage: www.elsevier.com/locate/measurement

Prediction of machining characteristics in coolant-assisted dry EDM of Inconel 625 and Titanium Grade 2 using Machine Learning

Jorge M. Cortés-Mendoza [a], Agnieszka Żyra [b,*], Horacio González-Vélez [a]

[a] Cloud Competency Centre, National College of Ireland, Mayor Street Lower, IFSC, Dublin 1, Ireland
[b] Cracow University of Technology, Faculty of Mechanical Engineering, al. Jana Pawła II 37, 31-864 Krakow, Poland

ARTICLE INFO

Keywords:
Dry Electro Discharge Machining (dry EDM)
Machine Learning (ML)
Inconel 625
Titanium Grade 2

ABSTRACT

Dry Electro Discharge Machining (dry EDM) is an eco-friendly alternative to conventional EDM. Its adoption in industrial applications is limited due to the difficulty of stabilizing and the complexity of the process. So, identifying proper input parameters is fundamental for improving the efficiency of this process, which can be used for machining hard-to-machine alloys. In this work, four Machine Learning (ML) approaches describe the correlation of the dry EDM process inputs and outputs with distilled water as coolant for Inconel 625 and Titanium Grade 2. To compare the machinability of these two materials the Palatnik index Ψ was introduced that depends on physical properties. The prediction models based on Linear Regression (LR), Random Forest (RF), Support Vector Regression (SVR), and Artificial Neural Networks (ANN) receive the independent variables, pulse time, current, voltage, and gas pressure, to estimate the Material Removal Rate (MRR), the relative percentage wear of the working electrode (EW), the working electrode velocity (v), and the surface roughness parameters (R_z and R_{sk}). It was found that ANN outperforms other ML approaches in prediction of MRR, v, R_z and R_{sk} in case of prediction accuracy while the material and its Palatnik index is taken into account as an input. In addition, in the case of prediction of EWR, RF, ANN outperforms and other ML approaches considering all the prediction accuracy criteria. The average efficiency of the models in prediction of testing data which were not contributed to training stage according to the R-squared values for MRR, EW, and v were 0.6735, 0.7955, and 0.7739. The main aim of the research was to reduce the experimental time to identify optimal input parameters with respect to the desired output parameters using ML.

1. Introduction

1.1. Problem statement

Green technology and sustainable manufacturing concepts changed the machining industry, intending to minimize the environmental impact, carbon footprint, and life cycles of material [1]. Dry Electrical Discharge Machining (dry EDM) is a step toward achieving the aforementioned concepts because it improves the process's sustainability with a gaseous medium instead of hydrocarbon-based dielectric. Despite its environmental advantage, dry EDM applicability is limited to machining small and micro-sized components due to its low material removal ability. In this context, several attempts have been made to enhance the Material Removal Rate (*MRR*) process by using external fields like ultrasonic and magnetic field assistance and rotation of electrode tubes. The results of these hybrid systems demonstrate relevant advances in the field in recent years.

On one hand, the application of a magnetic field in dry EDM shows a reduction in crater diameter and an increase in craters' depth [2]. Also, the magnetic field facilitates the expulsion of debris from the machining gap to enhance the process stability and increase the *MRR*, resulting in a smoother surface finish [3]. Furthermore, the magnetic field expands ionization at the inception of the spark, which reduces the ignition delay time but increases working Electrode Wear (*EW*). The pulsating magnetic field enables a greater thermal energy transfer to the workpiece due to its capacity to facilitate higher ionization and plasma confinement [4]. It improves the material removal mechanism and melting in dry EDM, which enhances geometric precision and the quality of the machined surface.

On the other hand, ultrasonic vibration of the workpiece also facilitates the removal of debris from the machining gap [5]. It also enhances process stability and augments the number of normal discharges while limiting the probability of arcs occurring [3]. High-speed rotation of the

* Corresponding author.
E-mail address: agnieszka.zyra@pk.edu.pl (A. Żyra).

https://doi.org/10.1016/j.measurement.2025.117966
Received 13 February 2025; Received in revised form 22 May 2025; Accepted 23 May 2025
Available online 25 May 2025

Nomenclature

AAD	Average Absolute Deviation
AAE	Average Absolute Error
ANN	Artificial Neural Network
DC	Discharge Crater
EDM	Electro Discharge Machining
EW	Working electrode wear
LR	Linear Regression
MAE	Mean Absolute Error
MAPE	Mean Absolute Percentage of Error
ML	Machine Learning
MRR	Material Removal Rate
MSE	Mean Square Error
PSO	Particle Swarm Optimization
RF	Random Forest
ReLU	Rectified Linear Unit
RMSE	Root Mean Square Error
RSM	Response Surface Methodology
SML	Supervised Machine Learning
SR	Surface Roughness
SSE	Sum of Squares Error
SVR	Support Vector Regression
TWR	Tool Wear Ratio
WE	Working Electrode

EW improves *MRR* and Surface Roughness (*SR*), but micro-cracks can appear during high-speed working electrode rotation [6,7]. However, establishing the aforementioned fields is not always possible because of the EDM machine's limitations and the sample size.

The combination of liquid and gas was a relevant advancement in the dry EDM field to improve the efficiency of the process and surface quality in terms of *SR* [8–12]. Although this type of machining is not employed in industrial applications, the development of dry EDM is a promising field of research in light of the significant size of the EDM market and the quantifiable environmental benefits. For example, the powder mixed near dry electrical discharge machining shows different *MRR* due to the thermal phenomena with diverse combinations of tool electrodes (brass and copper) and workpiece material [13].

Wet EDM exhibits the advantage of good machining stability at high discharge energy compared with near-dry EDM (kerosene and air mixture, deionized water and air mixture), consequently resulting in an improved *MRR* and *SR* concerning wet EDM [14,15]. Also, near-dry EDM milling is a stable finishing process to achieve a mirror-like surface finish [11]. This surface finish has a *SR* (R_a) value of 0.32 μm using a kerosene mist and a copper-infiltrated graphite electrode with low pulse energy. Moreover, a comparative study shows the difference between different dielectric (glycerin-air and water–air medium, and other bio dielectrics) [16,17]. The glycerin-air dielectric medium yields a higher *MRR* than the water–air dielectric medium with the same parametric settings. Finally, lower pulse duration and lower discharge current are key factors that influence the surface finish in near-dry EDM [18]. Also, nitrogen and helium gases can prevent electrolysis and provide a better surface finish in near-dry EDM.

Nevertheless, the valuable advantages of the dry EDM process with the presence of coolant cannot be easily assessed without considering the effects of some factors on the process performance measures. In other words, the multi-objective problem that describes this process should be optimized at the design stage to exploit the advantages of green EDM with a combination of gas and liquid. Consequently, a holistic model is required to facilitate the selection of an optimal setting that simultaneously maximizes production rate and product qualities. In recent years, several approaches have focused on predicting and modeling surface structure, roughness, and morphology after EDM. The following section presents several related works in the field.

1.2. Literature survey

In the literature, analytical, numerical, data-driven, and Machine Learning (ML) approaches for modeling EDM and dry EDM processes have been studied to predict and optimize some process characteristics. Analytical and numerical models mainly focus on predicting discharge craters, temperature distribution, and volume of material with lots of simplification [19–25]. Nevertheless, the obtained models aid the comprehension of the process, but they have many limitations, such as low prediction accuracy and extension to a reliable industrial problem.

Data-Driven Modeling (DDM) and ML are prediction methods that facilitate the correlation between the process inputs and outputs with high accuracy [26]. Several works in the state-of-the-art EDM use the statistical process of DDM to measure the effects of process factors over performance measures. In recent years, ML models have been extended to several domains due to their benefits, such as accelerating innovation, improving customer experience, and reducing costs. Here, we present relevant research in the domain of ML and EDM.

Khan et al. [27] encompass the utilization of Artificial Neural Networks (ANN) to predict *SR* (R_a) after EDM of titanium alloy. The efficiency of the ANN is measured using R-squared (R^2) and the Mean Square Error (*MSE*) metrics. The results show that the developed ANN is adequate for predicting *SR* because the predicted errors are within an acceptable range.

Bhandare and Dabade [28] develop an ANN to investigate the *MRR*, *EW*, and SR parameter (R_a) of Inconel 718 during dry EDM. The results show that an ANN with a 4-24-3 structure has the highest predictive accuracy for *MRR*, *EW*, and R_a performance measures. Also, they reveal an overall correlation coefficient of 0.94455, indicating a high degree of accuracy and effectiveness in the model and the ANN.

Ishfaq et al. [29] perform EDM machining of nickel-based superalloy with five biodegradable dielectrics (sunflower, amla, olive, mustard, and coconut oils). The results show a significant reduction in CO_2 emission compared to EDM performed in kerosene. The efficiency of the ANN model achieves an R^2 value greater than 0.9 and a reasonable prediction for Root MSE (*RMSE*). A multi-objective analysis based on a nonlinear optimization demonstrated that sunflower oil provides the optimal solution for the EDM process.

Quarto et al. [30] study ANN and Particle Swarm Optimization (PSO) models to improve the selection of optimal micro-EDM parameters. The authors use 134 cases to train and test an ANN, with 70–30 % division of the dataset. PSO identifies optimal process parameters with different multi-objective functions and constraints in the solution space. The results are validated with twelve micro-EDM tests to compare *MRR*, *EW*, and dimensional deviation. The method shows efficiency when constraints are fixed for the ANN inputs and the outputs respecting the imposed multi-objective function.

Sahayaraj et al. [31] employ the Radial Basis Function (RBF) and an ANN model to forecast the responses of *MRR* after the EDM process. The optimal architecture was determined through MATLAB by controlling the number of neurons and the number of hidden layers of the ANN. The results indicate that the Relative Error (*RE*) and the Sum of Squares Error (*SSE*) for the training and testing stages are 0.164 and 0.856, and 0.327 and 2.877, respectively.

Velpula et al. [32] investigate the impact of several input parameters on *MRR* and *EW* after EDM in oil using an ANN. The experimental results show that the ANN predicts *MRR* and *EW* with an accuracy of 0.93 and 0.94, respectively. It provides a reasonable methodology for predicting

the EDM process parameters.

Surya et al. [33] exanimate the machining characteristics such as R_a, *MRR*, and dimensional accuracy of Molybdenum after wire-EDM using an ANN. The results show that predicted values for the 70 % training set correlate highly with the measured values.

Kumat et al. [34] predict titanium alloy micro-hardness after cryogenic treatments and EDM processing based on several input parameters. Three grades of titanium alloy and three different electrodes are investigated during the experiment. The authors use an ANN to predict the material's micro-hardness. The results demonstrated a high correlation between microhardness's actual and predicted value.

Mondal et al. [35] use two types of predictive models for forecasting the *MRR* and *SR* after EDM using an ANN and the Response Surface Methodology (RSM) models. The results show that both models exhibit satisfactory accuracy, although the ANN-predicted model is more accurate. Also, the optimal input parameters for both models are reported.

Ganapathy et al. [36] investigate the correlation between ANN and RSM after EDM of unalloyed medium carbon (EN8) steel in EDM oil to predict *MRR*. The results show that the ANN-RSM approach is suitable for forecasting *MRR* according to R^2, *RMSE*, and Percentage of Average Absolute Deviation (*AAD*) for the RSM model. In contrast, the ANN model demonstrates a high proportion of R^2, RMSE, and AAD.

Kanake and Ahuja [37] explore the prediction of working *EW* during the micro-EDM process of stainless steel. The authors use ANN, Regression-Based Model (RBS), and Time-Series Moving Average (TSMA) model to predict working EW. MSE, RMSE, R^2, and Mean Absolute Percentage Error (MAPE) define the performance indicators to compare the efficiency of the methods. The results show that ANN provides better results in comparison with time-series and regression-based models with the highest coefficient of R^2 value.

Table 1 summarizes the reviewed literature for a better comprehension, it describes the main characteristics and parameters together with their methodologies and materials.

EDM is known as a chaotic process where nonlinear behavior and difficult-to-control nature based on the condition of material to be machined, dialectic and the main kinematic of the process. This is why majority of physics-based model or finite element simulations focused only on modeling of single discharge and spread it to a bigger scale to predict the main machining indicators. The problem will be more crucial when instead of liquid dielectric, gaseous medium is used where it causes expansion of plasma channel and changes the nature of the process. In this case developing a closed form model to predict the main process characteristics lacks to provide accurate results. This is why, in the present work, to address the issue, machine learning-based models have been developed based on the data derived from experiments to guarantee a precise prediction and forecasting the change of the main quality characteristics process under different processing condition. To achieve the best predictive models in term of accuracy, different machine learning approaches examined namely Linear Regression (LR), Random Forest (RF), Support Vector Regression (SVR), and artificial neural network (ANN) have been utilized to identify which of them meets the accuracy required for prediction of the external cooling assisted dry EDM's quality characteristics. Then performance of each approach was checked through different error criteria namely RMSE, MSE, R^2 and MAPE. Then, the model which has the best prediction

Table 1
Main characteristics of related works in the literature.

Model	Machine type	Parameters		Metrics	Material	Dielectric type	Working electrode	No. of trials	Ref.
		Input*	Output						
ANN	–	Pc, T_{on}, T_{off}, servo-vo	R_a	*MSE*, R^2	Titanium	–	Graphite	20	[27]
ANN	CNC EDM	Pc, T_{on}, vo, gaseous dielectric pressure	*MRR*, *TWR*, R_a	*MSE*	Inconel 718	Air	Cooper	27	[28]
ANN	–	Dielectric type, Cu powder in the fluid	*MRR*, *SR*, Energy Consumption	R^2, *RMSE*	Inconel 600	Sunflower, amla, olive, mustard, and coconut oils	Aluminium	15	[29]
ANN, PSO	Sarix SX-200 μEDM	Pc, vo, frequency, electrode diameter, wpm, elm	*MRR*, *TWR*, dimensional deviation	*RMSE*	Tungsten carbide, 304 steel, 316 steel	–	Brass	12	[30]
ANN	–	Pc, T_{on}, vo	*MRR*	*RE*, *SSE*	Eglin steel	kerosene	Tungsten	9	[31]
ANN	V3545 GRACE die sinking	Pc, T_{on}, T_{off}, tool lift	*MRR*, *EW*	–	17–4 PH Stainless Steel	Oil medium	Copper, Tungsten	25	[32]
ANN	CONCORD DK7720C CNC WED	Pc, T_{on}, T_{off}, bed speed	R_a, *MRR*, dimensional accuracy	*MSE*	Aluminium 7075	WEDM	Molybdenum	27	[33]
ANN	OSCARMAX S 645 EDM	Pc, T_{on}, T_{off}, dielectric type, tool material, wpm	Material hardness	*MSE*, R^2	Ti-5Al-2.5 Sn alloy Ti-6Al-4 V	Ferrolac 3 M EDM oil, Cryogenic treatment	Cooper, Chrome, tungsten	54	[34]
ANN	–	Pt, Discharge current, gap vo	*MRR*, *SR*	R^2	304 stainless steel	–	–	27	[35]
ANN, RSM	CNC EDM Grace V5030	T_{on}, discharge current, dielectric pressure, size of the tool	*MRR*	*AAD*, *RMS*, ER^2	EN 8 steel	EDM oil	Cooper	29	[36]
ANN, RBM, TSMA	DT-110i Hybrid Micro EDM	vo, capacitance, tool rotation speed	*EW*	*MSE*, *RMSE*, R^2	304 stainless steel	–	Brass	18	[37]
ANN	King ZNC K3200	Pc, Pd, electrodes' cryogenic process conditions	*EW*, *MRR*	R^2, *MSE*, *RMSE*, *MAPE*	AISI P20 tool steel	Petrofer dielectricum 358	Cooper, CuCrZr	176	[38]
LR, RF, SVR, ANN	Electro-discharge generator MATRIX MPS	T_{on}, velocity, current intensity, gas pressure, wpm	*MRR*, *EW*, R_z, R_{sk}, working electrode velocity (*U*)	R^2, *MSE*, *RMSE*	Inconel 625, Titanium Grade 2	Carbon dioxide with deionised water	Cooper	50	Ours

* The abbreviations for input parameters are pulse current (Pc), pulse time (Pt), pulse duration (Pd), pulse-on time (T_{on}), pulse-off time (T_{off}), workpiece material (wpm), electrode material (elm), and voltage (vo).

accuracy was utilized to navigate design space and find the impact of the process factors on main quality characteristics.

2. Materials and methods

2.1. Test stand and sample

Dry EDM with external workpiece cooling with deionized water in milling kinematics was performed on the dedicated research test stand equipped with an electro-discharge generator MATRIX MPS – 7163 160 V/3A [39], as shown in Fig. 1. A gaseous supply system expands the test stand to enable machining in a gaseous dielectric, where a thin-walled tubular electrode supplies carbon dioxide (gaseous dielectric) under pressure to the machining gap. Deionized water covering the workpiece ensures proper hearing dissipation from the machining area. The reason of selecting carbon dioxide as a dielectric medium was based on the satisfactory results of material removal rate, comparing to air-assisted machining, which was established during preliminary tests. It was found that while usage of carbon dioxide the formation of carbon layer improves the surface hardness, which has a positive influence on the material properties (increases the hardness of the white layer). The polarity of the electrodes was also established at the preliminary test stage (Fig. 2).

A single milling trial removed ten layers of material in two directions of the milling (in and out). The preliminary tests established the collection of ten layers of material while lowering the cutting electrode in each pass by 25 μm. They demonstrated that the machining conditions were stable when the number of material layers was reduced to ten.

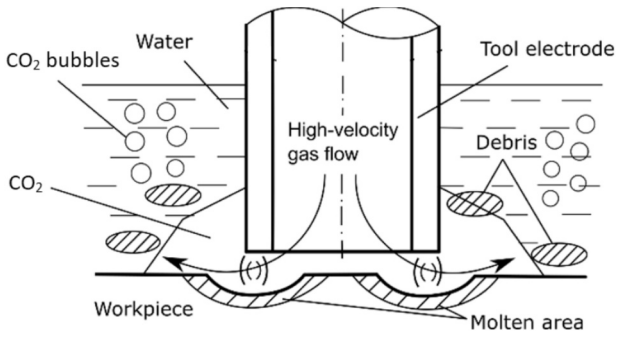

Fig. 2. Scheme of near-dry EDM milling in CO_2 with external workpiece cooling with deionized water [40].

The machined elements are two samples of Inconel (In) 625 and Titanium (Ti) Grade 2 with dimensions of 40.6 × 15.0 × 12.1 mm. Both materials are classified as hard-to-machine alloys with conventional machining methods. Table 2 shows the chemical composition of the materials based on a certificate provided by the manufacturer, and Table 3 describes the physical properties of both materials.

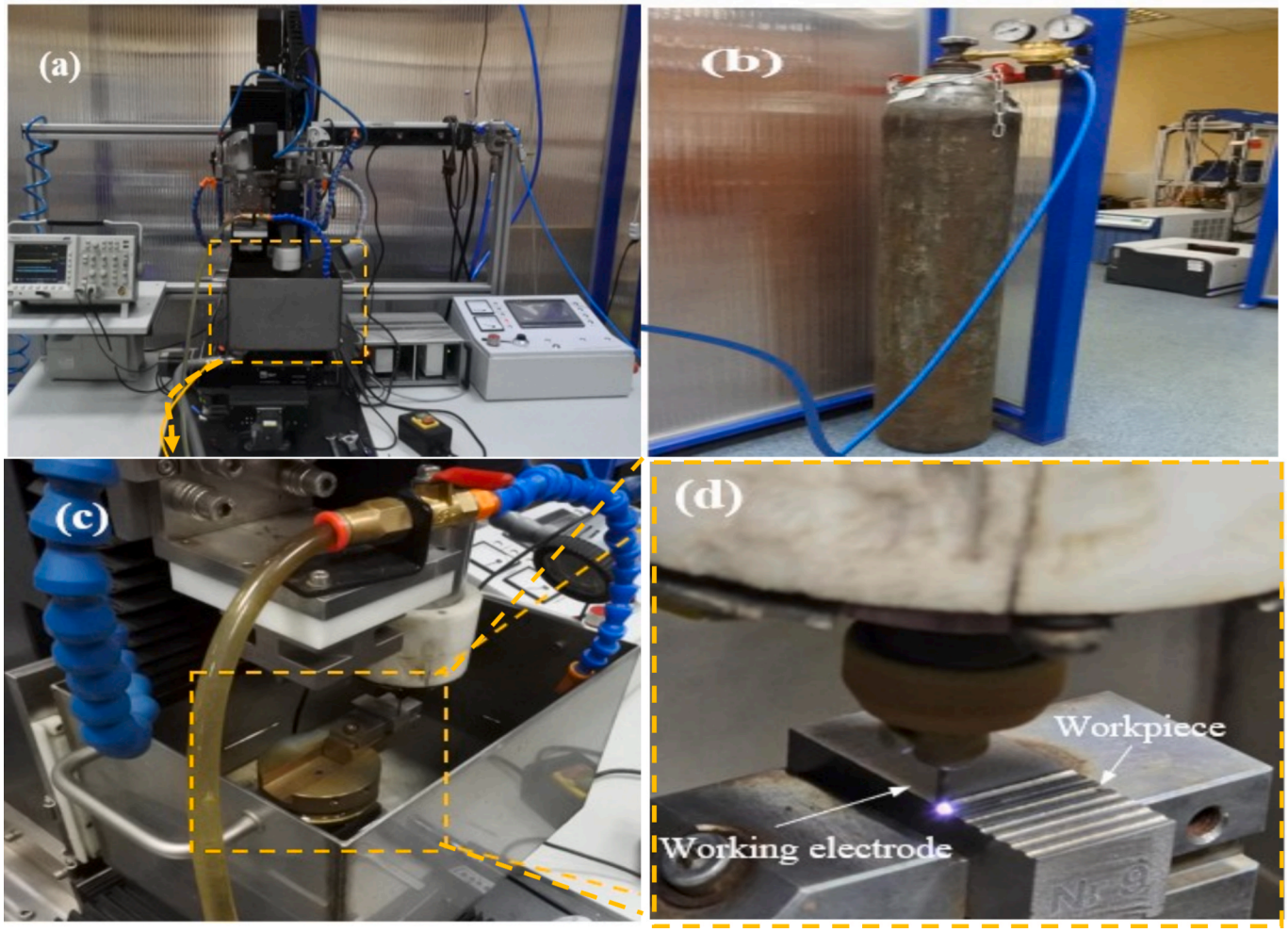

Fig. 1. Experimental test stand (a) main EDM machine modified for dry EDM (b) gas supplier and piping to the machine (c) dry EDM process (d) formation of spark in dry EDM in milling kinematics which machine grooves on the cubic workpiece.

Table 2
Certified chemical composition of Inconel 625 and Titanium Grade 2.

Material	Chemical composition						
Inconel 625	**Element**	**C**	**Si**	**Mn**	**P**	**S**	**Cr**
	Content (%)	0.013	< 0.05	< 0.02	< 0.005	< 0.0003	21.61
	Element	**Mo**	**Ni**	**Co**	**Ti**	**Al**	**Nb**
	Content (%)	8.20	63.58	< 0.050	< 0.02	0.17	3.34
Titanium Grade 2	**Element**	**Ti**	**Fe**	**C**	**N**	**O**	**H**
	Content (%)	99.50	≤ 0.17	≤ 0.03	≤ 0.028	≤ 0.17	≤ 0.10

Table 3
Physical properties of Inconel 625 and Titanium Grade 2.

Symbol	Property	Measurement unit	Inconel 625	Titanium Grade 2
ρ	Density	kg/m^3	8,442	4,510
θ_m	Melting point	K	1,621	1,933
c	Specific heat	J/kg·K	410	520
λ	Thermal conductivity coefficient	W/m·K	9.8	20.8
Ψ	Palatnik' index	–	8.91×10^{13}	18.2×10^{14}

2.2. Experimental plan

Tests followed the central composition research plan based on the response surface methodology. The total of 25 experiments considers the four-factor test plan according to pulse on time (t), voltage (U), current intensity (I), and gas pressure (p). The test in the center of the research plan, with the configuration $t = 300\,\mu s$, $U = 100V$, $I = 2.7A$, and $p = 6bar$, was repeated three times. Table 4 presents the ranges of variation in the input parameters.

The value ranges for parameters were defined based on their efficiency, stability, and limits of hardware:

- t values below 100 μs would be ineffective, and above 500 μs could result in a potential loss of machining stability,
- U variations are limited by the generator used during the tests,
- 3 I Values lower than 0.9 A would be inadequate for machining hard-to-machine materials, and higher 4.5 A could result in excessive energy being generated during discharge
- p variations are related to the limits of the CO_2 reducer used.

Tables 5 and 6 show the variable input parameters of the experimental plan and the constant machining parameters.

Additionally, the Palatnik criterion is employed to ascertain the EDM machinability level of a given material. It posits that thermal phenomena exert the most significant influence on material removal during EDM machining. More accurately, the Palatnik constant corresponds to machinability of material while being processed by thermal erosion based process like EDM or laser machining. Based on this coefficient, the material with higher Ψ is more difficult-to-cut that means further time and energy are required to remove material from the relevant papers. There also other literatures which use this physical quantity to identify and justify machinability of thermal-based material removal process. To quantify this effect, it is defined by using the following relationship [41–43]:

$$\Psi = c^*\rho^*\lambda^*(\theta_m)^2$$

where:
$c[J/(kg{\cdot}K)]$- specific heat,
$\rho[kg/m^3]$- density,
$\lambda[W/(m{\cdot}K]$- thermal conductivity coefficient,

Table 5
Variable input parameters of the experimental plan.

Symbol	Parameter	Values
t	Pulse on time	100–500 μs
U	Voltage	80–120 V
I	Current intensity	0.9–4.5 A
p	Gas pressure	2–10 bar
Ψ	Palatnik's index	8.91×10^{13} (Inconel 625) 18.2×10^{13} (Titanium Grade 2)

Table 6
Constant machining conditions during tests.

Parameter	Values
Working Electrode (WE)	Thin-walled Cooper pipe
WE outer diameter	∅1 mm
WE inner diameter	∅418 μm
Gas medium	Carbon dioxide
Pulse duty factor (η)	0.5
External workpiece cooling medium-type	Deionized water
Electrical conductivity (G)	0.01 μS
Removed material layers per trial	10
Kinematics of WE movement	Milling

Table 4
Input parameters during dry-EDM with coolant.

Trial number	t[μs]	U[V]	I[A]	p[bar]	Trial number	t[μs]	U[V]	I[A]	p[bar]
1	200	80	1.8	4	14	400	120	1.8	8
2	200	80	1.8	8	15	400	120	3.6	4
3	200	80	3.6	4	16	400	120	3.6	8
4	200	80	3.6	8	17	100	100	2.7	6
5	200	120	1.8	4	18	500	100	2.7	6
6	200	120	1.8	8	19	300	100	0.9	6
7	200	120	3.6	4	20	300	100	4.5	6
8	200	120	3.6	8	21	300	100	2.7	2
9	400	80	1.8	4	22	300	100	2.7	10
10	400	80	1.8	8	23*	300	100	2.7	6
11	400	80	3.6	4	24*	300	100	2.7	6
12	400	80	3.6	8	25*	300	100	2.7	6
13	400	120	1.8	4					

* Three repetitions in the center of the research plan.

$\theta_m[K]$- melting point.

Palatnik index indicates the EDM machinability property of the material, a higher value describes a more challenging material for machining. A high conductivity of the workpiece material indicates a rapid dissipation of the heat generated by the electrical discharge, resulting in a reduced volume of removed material. An increase in thermal conductivity results in a reduction in the electro-erosion machinability of the material. According to Palatnik's criterion, the EDM machinability of a material is inversely proportional to the square of its melting temperature. Therefore, the melting point is a primary factor influencing the material's machinability. Certainly, the aforementioned criterion does not consider properties that can affect the EDM machinability of materials, such as the latent heat of fusion or the latent heat of vaporization. Latent heat describes the amount of energy released or absorbed by a material during a change of state or phase transition. Materials with a high latent heat require a greater amount of heat to be melted or vaporized, which can manifest as a reduction in the EDM machinability of the material [41].

According to the aforementioned discussion, it can be stated that the Palatnik index provides an important characteristic to the prediction models based on ML. To justify the significant differences between the two materials in terms of parameter significance, the interaction of process factors with materials on main EDM machinability indicator i.e. MRR that is extremely important in the case of dry EDM process has been studied and shown in Fig. 3. According to this figure, it is seen that the change of material following the Palatnik index significantly impacts the variation of MRR. In all the provided graphs, it is evident that the MRR of the Inconel 625 irrespective to the process factors are higher than Ti Grade 2. This can be justified that the Inconel has the lower value of Palatnik index i.e. 8.91E13, compared to titanium grade 2 that its Palatnik index is 18.2E13.

Moreover, according to the Fig. 3a, it is seen that irrespective to the type of material being machined, the MRR decreases by increasing the pulse time, that can be attributed to expansion of plasma channel during discharges that significantly reduces the energy density and causes MRR to be reduced. Also, from the Fig. 3b, it is seen that for both of Inconel and Ti Grade 2, the MRR increases by voltage that is due to increasing the discharge energy which causes melting and evaporation of more material and subsequently higher MRR. Similar scenario is observed in Fig. 3c in variation of MRR by current intensity that can be also attributed to further energy input and more removed material.

Effect of gas pressure on variation of MRR for different material has been shown in Fig. 3d. Accordingly, it is observed that for Inconel material, the MRR adopts higher values while gas pressure increases. It can be attributed to the fact that the cooling efficiency of the Inconel improves at further gas intake pressure which prohibits the Inconel to be resistant against material removal action [44]. But the scenario is different in the case of Ti Grade 2, by increasing the pressure of the coolant, the MRR decreases. It can be stated that the EDM is a thermal based erosion process; hence, when the cooling pressure goes beyond a critical values and becomes excessive, the thermal efficiency of process is deteriorated and results is reduction of heat input; accordingly, the MRR decreases. In this case, the high interaction between the material and the process factor is dramatically significant.

3.1. Measurement of outputs

The main performance measure of the process, along with methodologies adopted for the measurement and quantification of these outputs, can be found as follows:

- Material Removal Rate (*MRR*),
- Relative percentage wear of the working electrode (*EW*),
- Working electrode velocity (*v*),

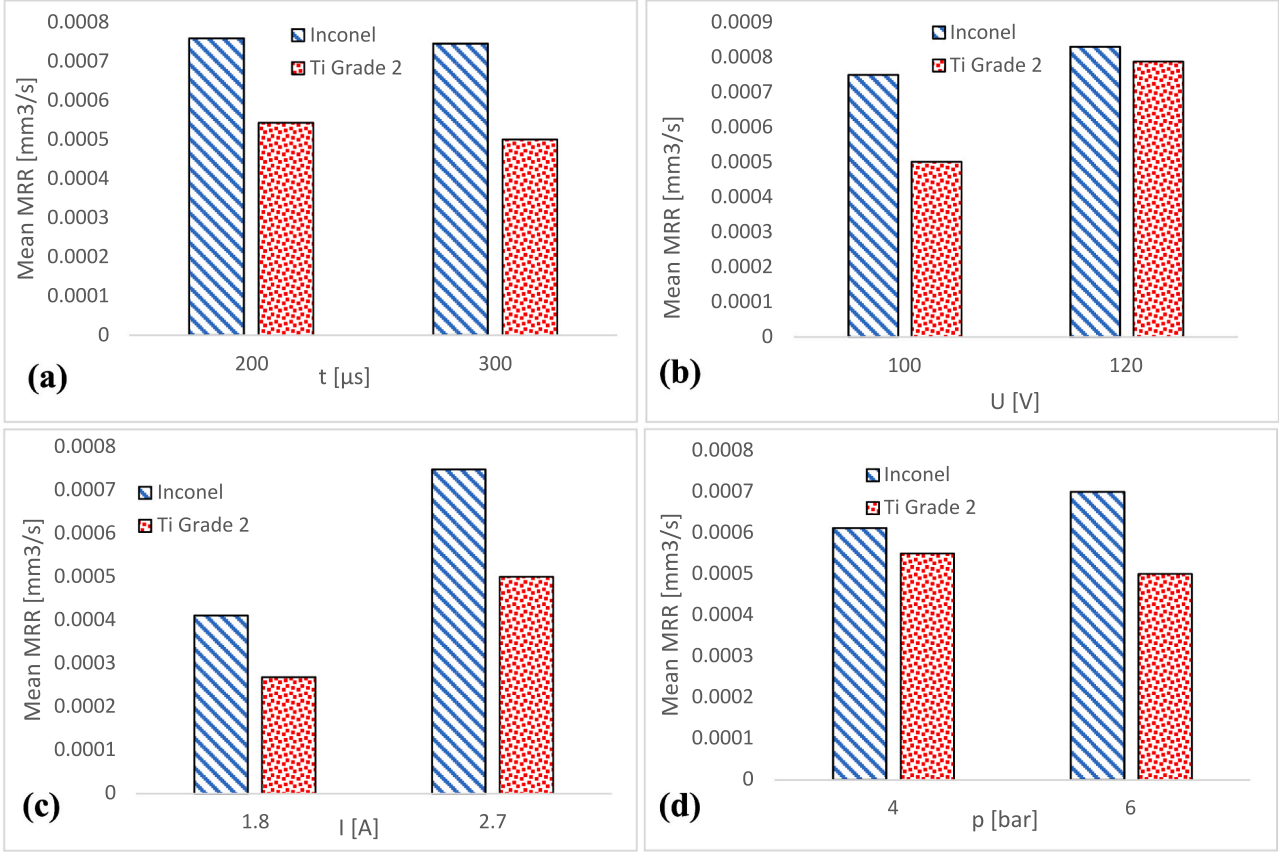

Fig. 3. The impact of process factors on MRR for different type of material (a) Pulse on time (b) Voltage (c) Current intensity (d) Gas inlet pressure.

- SR parameters: R_z and R_{sk}.

The EDM milling efficiency was determined by calculating the volume of material removed and the total milling time in each trial, with ten layers of material collected at each time point. A cross-section is trapezoidal in shape as a consequence of the wear observed on the side surface of the working electrode, Fig. 3 illustrates the cross-section of a single groove. Given that the milling was conducted in two directions, it was deemed appropriate to measure the groove height (c) and width (b) on three occasions at the entrance and exit of the electrode, respectively, and to measure the groove width (a) on three occasions. The results were subsequently averaged.

The volume of material removed (V_m) in a single sample was determined by the formula:

$$V_m = \frac{(b+a)}{2} \bullet c \bullet l$$

where l is the sample length.

The idea of measuring the width and height of the grooves is illustrated in Fig. 4. The measurements were obtained using an Olympus optical microscope with Olympus Stream software.

The *MRR* value is calculated according to the formula:

$$MRR = \frac{Vm}{t},$$

where t is the total machining time per trial.

The relative percentage wear of the working electrode is calculated as follows:

$$EW = \frac{Ve}{Vm} \cdot 100\%,$$

where Ve is the volume of working electrode material removed per trial.

The average working electrode velocity during milling was determined according to the formula:

$$v = \frac{L}{T},$$

where milling length L is the length of the sample section to be processed multiplied by the number of material layers to be collected and T represents the total milling time of ten layers of material during one test, this was determined in specific tests.

The roughness measurements of selected roughness parameters (R_z and R_{sk}) were obtained using a Taylor Hobson profilometer with a measuring section length of 13 mm. For each surface, the roughness value is the average of three roughness measurements taken at distinct locations. The reasons for choose of Rsk together with Rz is that the EDM is a chaotic process which generates the surface randomly based on the numbers of discharge craters which are formed during machining. The roughness indices Rsk greatly shows this random generation of roughness that is main goal of our work which seeks for how the process parameters in dry EDM impacts the asymmetrical formation of surface topography.

The combined results for Material Removal Rate (*MRR*), Relative percentage wear of the working electrode (*EW*), Working electrode velocity (v), SR parameters: R_z and R_{sk} for both Inconel 625 and titanium Grade 2 are presented in the Table 7.

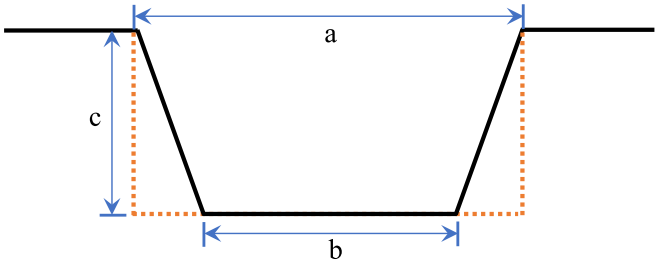

Fig. 4. Cross-section of a single groove with measured values.

3.2. Statistical analysis

The experimental results underwent statistical analysis to investigate potential correlations between input and output factors. Tables 8 and 9 summarize the Pearson correlation coefficients (r) between the analyzed input and output variables for Inconel 625 and Titanium Grade 2, respectively. The analysis does not consider interactions between input variables, which will be considered when assigning responses.

Analysis of significance of parameters based on the Pearson method talking about coefficient of determination i.e. R^2 [45] categorizes the correlation to "uncorrelated", "weak-correlated", "average-correlated", "strong-correlated" and "very strong correlated" where the absolute values of correlation coefficient are in ranges of "0–0.2", "0.2–0.4", "0.4–0.7", "0.7–0.9" and "0.9–1", respectively. On the basis of this definition, it can be stated that the prediction accuracy of the models which falls between the range of 0.7 to 1 are satisfactory that can navigate the design space. It needs to be noted that addition of the data might increase the R^2 values, however, it doesn't guarantee prediction accuracy. This is why in the presented work, different metrics were used to analyze the accuracy of ML algorithms in prediction of dry EDM characteristics.

According to the Tables 8 and 9, it is seen that the most significant parameter for MRR and R_z is current intensity, and for the EW, correlation coefficients are either uncorrelated or weakly correlated except the gas pressure in case of machining of Titanium alloy that is known as average-correlated parameter. Also, similar scenario exists for R_{sk} where factors found uncorrelated or weakly correlated for both materials.

It is interesting that nevertheless the current intensity is found as significant parameter on R_z, it is a weak corelated parameter for R_{sk}. This can be referred to definition of R_{sk} and R_z while processing by EDM. As the nature of EDM process is chaotic and it doesn't follow defined distribution of roughness, formation of symmetrical pattern that is repeated with a given frequency in line with cut-off length rarely happens. Therefore, it can be said that R_{sk} doesn't significantly vary by EDM process parameters. However, R_z is the average of five distances between the peaks and valleys that can be adjusted by formation of discharge craters in EDM process.

4. Machine learning modeling

Machine Learning (ML), a subfield of Artificial Intelligence, focuses on developing and studying statistical algorithms that can learn from data and generalize the knowledge to unseen data. Recently, several ML algorithms have surpassed many previous approaches in performance. For this reason, ML algorithms have been incorporated in different fields, including transportation, image processing, education, agriculture, business, medicine, and industry [46] (see Section 2).

Supervised ML (SML) is one of the four main categories of ML algorithms that uses labeled datasets to train the algorithms. If the main goal of the prediction task is a discrete target variable, then the algorithm affronts a classification problem. The problem is considered a regression problem under a target continue variable. In the present work, number offour ML algorithm namely Linear regression (LR), artificial neural network (ANN), Random Forest (RF) and Support Vector Regression (SVR) have been used to correlate a mapping relationship between the input and output of dry EDM process in presence of water-cooling. The description of each network and the implementation of corresponding algorithm have been presented as follows:

4.1. Linear Regression

Linear Regression (LR), an SML algorithm, computes the linear

Table 7
Experimental results of MRR, EW, v, R_z and R_{sk} from Titanium Grade 2 and Inconel 625.

Trial no.	Titanium Grade 2					Inconel 625				
	MRR[mm^3/s]	EW [%]	V [mm/s]	R_z [μm]	R_{sk} [μm]	MRR [mm^3/s]	EW [%]	V [mm/s]	R_z [μm]	R_{sk} [μm]
1	0.000106	2.160	0.010	15.22	−0.38	0.000217	3.461	0.029	20.10	0.24
2	0.000227	0.106	0.012	11.48	0.78	0.000367	3.892	0.047	24.73	0.24
3	0.000528	0.322	0.031	23.00	−0.06	0.000725	3.364	0.083	20.67	0.06
4	0.000872	0.090	0.052	17.21	0.06	0.000804	2.902	0.104	27.67	0.02
5	0.000169	0.897	0.010	16.22	−0.31	0.000446	4.706	0.054	16.97	0.25
6	0.000312	0.751	0.017	21.60	0.07	0.000559	3.820	0.077	18.97	0.19
7	0.000857	0.934	0.042	26.58	0.15	0.001262	4.100	0.139	23.60	0.37
8	0.001276	0.307	0.060	26.29	0.60	0.001691	5.202	0.167	23.17	0.10
9	0.000174	1.049	0.010	16.47	−0.28	0.000315	3.769	0.046	20.00	0.38
10	0.000478	0.176	0.024	16.28	−0.04	0.000382	3.680	0.104	12.53	0.15
11	0.000959	0.159	0.044	22.24	−0.15	0.000699	4.112	0.118	29.23	0.57
12	0.001491	0.046	0.068	13.96	0.36	0.001068	6.294	0.110	29.37	0.53
13	0.000368	3.001	0.027	14.30	0.75	0.000475	4.336	0.076	16.63	0.37
14	0.000323	1.185	0.023	19.71	0.23	0.000529	5.872	0.104	16.30	0.11
15	0.001274	0.890	0.076	21.08	0.78	0.000758	4.934	0.116	26.50	0.06
16	0.001721	0.355	0.102	18.63	0.40	0.000910	6.741	0.116	25.70	−0.13
17	0.000375	0.476	0.021	20.02	−0.04	0.000597	5.234	0.083	20.53	0.72
18	0.000857	0.152	0.043	16.99	−0.30	0.000829	5.164	0.110	19.23	−0.06
19	0.000267	0.745	0.028	12.46	−0.87	0.000091	12.016	0.020	11.43	0.48
20	0.002085	0.113	0.094	14.82	−0.07	0.001433	6.646	0.192	29.20	−0.04
21	0.000279	2.834	0.022	20.16	−0.15	0.000459	5.257	0.067	21.57	0.10
22	0.000749	0.000	0.036	15.68	−0.77	0.000729	6.251	0.143	29.30	0.20
23	0.000518	0.919	0.026	26.61	0.05	0.000689	4.321	0.149	19.80	−0.15
24	0.000527	0.000	0.025	19.37	−0.20	0.000694	6.398	0.119	36.03	0.23
25	0.000483	0.184	0.030	18.09	0.69	0.000650	3.129	0.145	16.13	0.14

Table 8
Correlation coefficient values between the analyzed dependent and independent variables for Inconel 625.

Variable	*MRR*[mm^3/s]	*EW*[%]	R_z[μm]	R_{sk}[μm]
***t*[μs]**	−0.053	0.182	−0.015	−0.180
***U*[V]**	0.284	0.226	−0.139	−0.196
***I*[A]**	**0.827**	−0.148	**0.658**	−0.252
***p*[bar]**	0.221	0.170	0.140	−0.161

Table 9
Correlation coefficient values between the analyzed dependent and independent variables for Titanium Grade 2.

Variable	*MRR*[mm^3/s]	*EW*[%]	R_z[μm]	R_{sk}[μm]
***t*[μs]**	0.271	0.032	−0.208	0.060
***U*[V]**	0.143	0.259	0.346	0.272
***I*[A]**	**0.831**	−0.375	**0.421**	0.272
***p*[bar]**	0.254	**−0.605**	−0.190	0.067

relationship between the dependent variable and independent features by fitting a linear equation to the observed data. The goal of LR is to find an equation that minimizes the error between the predicted and actual values with respect to the training dataset of N instances with d features. The multiple linear regression model takes the form [46]:

$$Y = f(X) + \epsilon = \widehat{\beta}_0 + \widehat{\beta}_1 x_1 + \cdots + \widehat{\beta}_d x_d + \epsilon$$

where ϵ describes the disturbance term or error variable,$x_1, x_2, \cdots, x_d$ the features of an instance X, and $\widehat{\beta}_0, \widehat{\beta}_1, \cdots, \widehat{\beta}_d$ the regression coefficients.

The Residual Sum of Squares (RSS) measures the level of variance in the error term, or residuals, of the model as [46]:

$$RSS = \sum_{i=1}^{N} (Y_i - f(X_i))^2$$

where Y_i defines the observed value, $f(X_i)$ is the predicted value by the linear approximation, and X_i the explanatory variable for $i = 1, \cdots, N$.

Fitting a linear model to a given dataset requires estimating the regression coefficients $\widehat{\beta}_0, \widehat{\beta}_1, \cdots, \widehat{\beta}_d$ such that ϵ is minimized. The training phase of LR finds the line with the coefficients $\widehat{\beta}_0, \widehat{\beta}_1, \cdots, \widehat{\beta}_d$ that minimize *RSS*.

Fig. 5 [46] shows an example of prediction with a simple LR where blue dots are the instances of the dataset used to create the (red) linear model, also known as the training dataset. The error ϵ is the difference between the observed value Y (orange dot) of the input of X and the predicted value $f(X) = \widehat{\beta}_0 + \widehat{\beta}_1 x_1$ (black dot).

According to the definition, the linear regression models for the correlating the process inputs to outputs have been defined as follows:

$$MRR = -0.13441143x_1 - 0.062055x_2 + 0.077938x_3 + 0.105832x_4 + 0.617859x_5 + 0.179875x_6$$

$$Ew = -0.08057508x_1 - 0.706865x_2 + 0.109636x_3 + 0.133243x_4 - 0.075969x_5 - 0.078176x_6$$

$$v = -0.02199991x_1 - 0.647117x_2 + 0.104774x_3 + 0.154047x_4 + 0.548398x_5 + 0.162842x_6$$

$$Rz = 0.05469054x_1 - 0.399168x_2 - 0.091395x_3 + 0.135280x_4 + 0.501958x_5 + 0.058769x_6$$

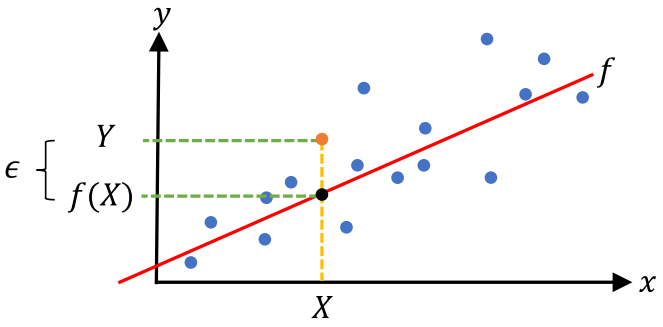

Fig. 5. Example of a simple LR.

$$Rsk = 0.09476015x_1 + 0.040164x_2 + 0.093982x_3 + 0.057728x_4 - 0.117807x_5 + 0.106405x_6$$

4.2. Random Forest

An alternative nonlinear approach consists of dividing or partitioning the space into smaller regions where the interactions are more manageable. Recursive partitions of the space generate chunks so tame for creating simple models for them. A prediction tree uses a tree to represent the recursive partition; the tree's structure defines the partitions. A Decision Tree (DT), an SML algorithm, creates a model that predicts the value of a target variable by learning simple decision rules inferred from the data features. A DT represents a function f that takes a vector of feature values as input and returns a decision value, where the nodes in the DT represent the features of the dataset. The leaves characterize the values to estimate the regression value [46].

Fig. 6 shows an example of a DT with two features (x_1 and x_2) and its partitioning of the space, the three thresholds ($x_1 \leq 3$, $x_2 \leq 2$, and $x_1 \leq 5$) generate four terminal nodes or regions in the space (R_1, R_2, R_3, and R_4). The value in each region is the mean of the response for the observations that fall there. The prediction of X is equal to the value of R_3 which consists of the average value of all the points within $3 < x_1 \leq 5$ [47].

The goal of the training phase of DT is to find the thresholds or cuts that create the regions that minimize the Mean Squared Error (MSE) [46]:

$$MSE = \frac{1}{N}\sum_{i=1}^{N}(Y_i - f(X_i))^2$$

The prediction function f is specified by:

$$f(X) = \sum_{j=1}^{J} w_j \left\| (X \in R_j) \right.$$

where J is the total of leaves in the DT, R_j defines the region of the j-th leaf node, the binary indicator function:

$$\left\| (e) = \begin{cases} 1 if e is true \\ 0 if e is false \end{cases} \right.$$

and w_j establishes the predicted output of the j-th leaf node by:

$$w_j = \frac{\sum_{i=1}^{N} Y_i \left\| (X_i \in R_j) \right.}{\sum_{i=1}^{N} \left\| (X_i \in R_j) \right.}$$

Random Forest (RF) is an ensemble learning algorithm that creates several DTs as a single model, and its output prediction is based on the mean of their trees to correct for the individual trees' tendency to overfit the data. RF ensures low correlation among decision trees by generating a random subset of features. The RF algorithm randomly selects a sample of data in a training set with replacement (one instance of the dataset can be chosen more than once) and a subset of features to create an uncorrelated forest of DTs. Fig. 7 shows an example of an RF with three DTs and an averaging of the results. The prediction $f(X)$ of Y for X is the average value of the outputs provided by the three DTs in the RF [46].

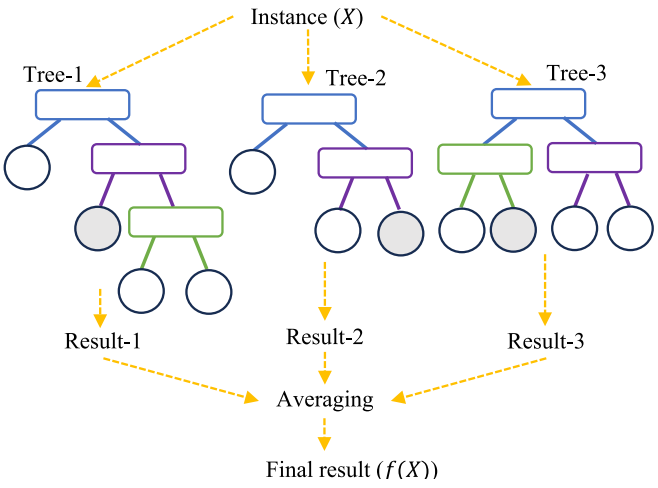

Fig. 7. Example of an RF with Three DTs and averaging.

4.3. Support Vector Regression

Support Vector Regression (SVR), an SML algorithm, defines a region around the function that can be approximated with a certain tolerance. The tube region aims to find the best approximates of the continuous-valued function where the points inside the tube are considered correct predictions, minimizing the prediction error. Kernel functions of SVR project original data into high-dimensional feature spaces where linear or more complex relationships may exist, helping to deal with nonlinear processes. Some advantages of SVR are good performance with multidimensional data, the advantage of high-dimension count datasets, and the fact that it is not a resource-hungry algorithm [46].

The ε-insensitive loss function in SVR assigns zero prediction error to the points that lie inside the ε-tube, where ε value defines the margin width where data points are correctly predicted. The objective of SVM is to find the optimal coefficients $\hat{\beta}_0, \hat{\beta}_1, \cdots, \hat{\beta}_k$ such that errors in the prediction are lower than ε. Slack variables ξ and ξ^* create a soft margin that allows for the measurement of errors, making the optimization feasible. The SVM optimization problem has the form [46]:

$$\min \frac{1}{2}\sum_{j=1}^{d} \hat{\beta}_j^{\,2} + C\sum_{i=1}^{N}(\xi_i + \xi_i^*) s.t. \begin{cases} Y_i - f(X_i) \leq \varepsilon + \xi_i \\ f(X_i) - Y_i \leq \varepsilon + \xi_i^* \\ \xi_i + \xi_i^* \geq 0 \end{cases}, \forall i \in \{1, 2, \cdots, N\}$$

where the constant $C > 0$ defines a trade-off between the flatness of f and the toleration of deviations larger than ε.

Fig. 8 shows an example of univariable SVR with values of the

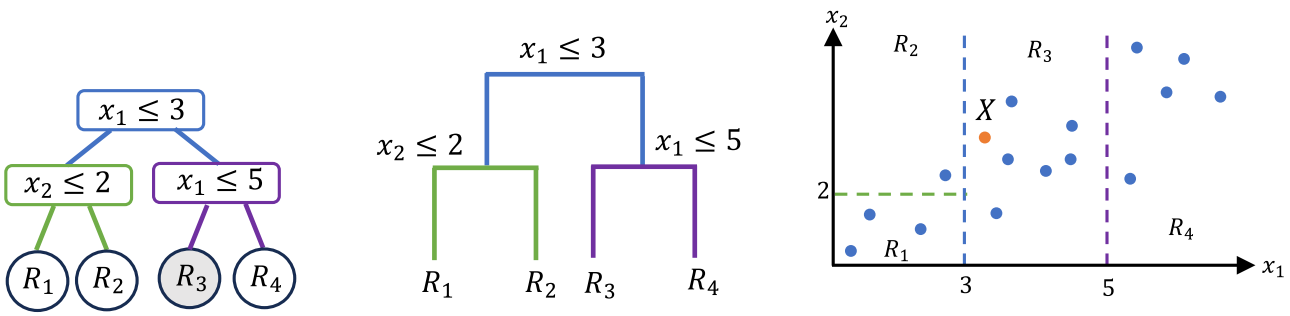

Fig. 6. Example of DT graphical representation and the partitioning of the space according to the leaf nodes.

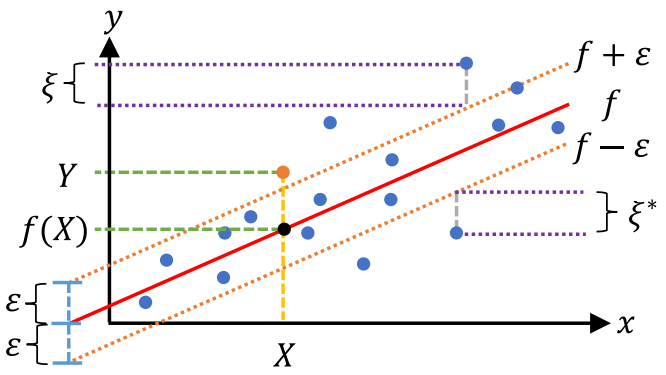

Fig. 8. Example of univariable SVR.

prediction function f are found using the training dataset, where the orange lines define the ε-tube, and the purple lines show the measurement of slack variables ξ and ξ^*. Also, the difference between the prediction value $f(X)$ and the current value Y of the instance X for the final model.

4.4. Artificial Neural Networks

Artificial Neural Networks (ANN), an SML algorithm, simulates the human brain's functionality where interconnected neurons provide the structure to solve problems. The network organizes neurons on independent layers with an arbitrary number of them [48]. ANNs can create straightforward, highly accurate models for complex problems [49]. A mathematical model of a neuron consists of a linear combination of inputs and an activation function. Fig. 9 shows the basic structure of the artificial neuron, where x_0 defines a bias value, $x_1, x_2, \cdots, x_k$ are the features of an instance in the dataset, $w_0, w_1, w_2, \cdots, w_k$ corresponds to the weights of the inputs, and f is the activation function.

Neurons are connected by edges and organized into layers to create ANNs. Layers have different functionalities: The input layer receives the external signals, hidden layers are intermediate layers that process the information, and the output layer produces the output. Fig. 10 shows an example of ANN with three layers: an input layer with two neurons, a hidden layer with three neurons, and an output layer with two neurons [46].

The training process finds the best values of the weights for each neuron in the ANN, they minimize the error in the prediction of the output using *MSE*. Initially, the ANN assigns random weights to each edge. Then, the ANN estimates the output for the instances in the training dataset, and the error between the actual and expected outputs is computed. Finally, the backpropagation algorithm adjusts the weights

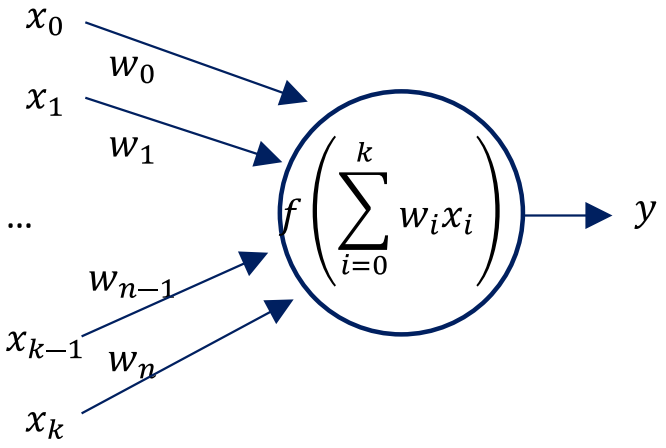

Fig. 9. Mathematical model of a Neuron.

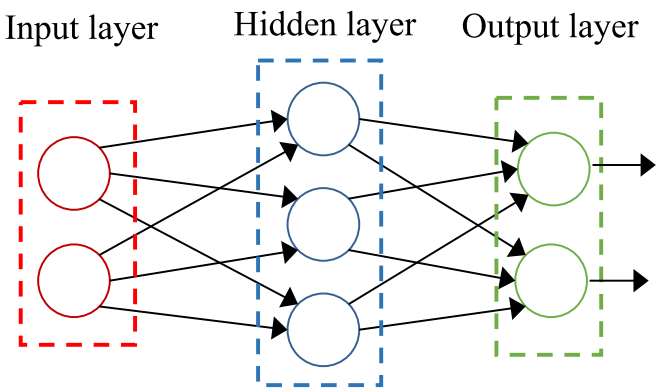

Fig. 10. An ANN with three layers and seven neurons (2-3-2).

of all edges to minimize the *MSE*. This process is repeated during several epochs to keep updating the weights until the network works properly. Some important limitations for the development of an ANN are the definition of the structure (the number of layers and neurons per layer and the internal structure, connections between layers) and the training process (number of epochs, activation function, learning rate, among others) [46].

4.5. Implementation of ML algorithms

This section presents the performance comparison of LR, RF, SVR, and ANN to predict *MRR*, *EW*, v, R_z, and R_{sk}. The implementation based on Python 3.12, and sklearn 1.4.1 library is performed on a computer with 64-bit Windows 11 Pro, Intel(R) Core (TM) i9-10980XE CPU at 3.00 GHz, 64 GB of memory, and 2 TB SSD.

4.5.1. Prediction model

In the preliminary phase of the study two prediction models were developed for each of the ML approaches. The first prediction model was trained only with dataset for one machined material, and the second prediction model was trained using the information about both machined materials. The output of both prediction models was only one value of *MRR*, *EW*, v, R_z, and R_{sk}. It was found that better performance is achieved when training model with using the information about both machined materials. That is why only one prediction model was reported in the study. Fig. 11 shows the inputs and outputs of the proposed prediction model for the four ML approaches. The model receives Palatnik's index (which characterizes the type of material) as an additional input.

4.5.2. Datasets

Evaluating the strategies with real data is fundamental to measuring their performance. Two datasets with a series of integer and continuous input variables and continuous output values were considered. Table 10 shows the characteristics of the input values for both datasets.

All the features' values are standardized using a method of feature scaling. The standardization process centers data around a mean of zero

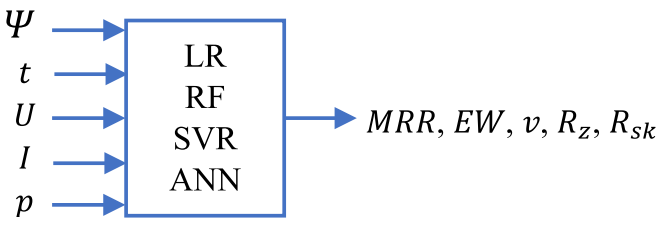

Fig. 11. Input and output parameters of the proposed prediction models for the four ML approaches.

Table 10
Input values of Inconel and Titanium datasets.

Input	Values
Ψ	{8.91, 18.2}
t	{100, 200, 300, 400, 500}
U	{80, 100, 120}
I	{0.9, 1.8, 2.7, 3.6, 4.5}
p	{2, 4, 6, 8, 10}

and a standard deviation of one to avoid some features dominating others due to their magnitudes. Fig. 12 presents statistical information about the datasets after the standardization. Several outliers were identified and removed to avoid a reduction in the quality and accuracy of the ML models. Also, there is a lack of sufficient representation of subgroups within the data, so they were removed to avoid any bias in the models.

The Simple Split technique provides a methodology to compare the LR, RF, SVR, and ANN performance. The dataset was randomly divided into two subsets with a number of instances: training and testing. The training set was used to train the classification model, and the testing set was used to verify the training process. Table 11 shows the number of instances in each training dataset.

4.5.3. Metrics

Four standard metrics were considered to evaluate the efficiency of the predictive model. They are mean square error (MSE), root mean square error (RMSE), R^2 and mean absolute percentage of error (MAPE). Their definition can be expressed as follows:

$$MSE = \frac{1}{N}\sum_{i=1}^{N}(y_i - \hat{y}_i)^2, \tag{1}$$

$$RMSE = \sqrt{MSE}, \tag{2}$$

$$R^2 = 1 - \frac{\sum_{i=1}^{N}(\hat{y}_i - y_i)^2}{\sum_{i=1}^{N}(\bar{y}_i - y_i)^2}, \tag{3}$$

$$MAPE = 100\frac{1}{N}\sum_{i=1}^{N}\left|\frac{y_i - \hat{y}_i}{y_i}\right|, \tag{4}$$

where y_i defines the observed value, $\hat{y}_i$ is the predicted value, and $\bar{y}_i$ specifies the mean y_i value for $i = 1, \cdots, N$.

4.5.4. Configuration

Proper parameters (configuration) of the strategies are fundamental to optimize their performance. Hyperparameters are external configuration variables that control the learning process of the ML model during its training. Hyperparameter optimization finds values of the parameters that optimize the model by minimizing a predefined loss function on given test data. The models with the best performance according to *MSE*, *RMSE*, and R^2 for predicting *MRR*, *EW*, *U*, R_z, and R_{sk} are used to measure their efficiency on the testing dataset with unseen data. Those values are reported in the results section.

The hyperparameters for RF include the number of decision trees in the forest (n_estimators), the maximum depth of the tree (max_depth), the minimum number of samples required to split an internal node (min_samples_split), and whether bootstrap samples are used when building trees (bootstrap).

Table 12 presents the grid values to define the best hyperparameters of the RF with 5-fold Cross-Validation (5CV) using the training dataset. These values were set to avoid overfitting due to the limited number of instances in the dataset. Table A1 shows the configuration of the best strategies found during the simulation, see Appendix A.

The hyperparameters for SVR are the kernel type, the degree of the polynomial kernel function, the epsilon value, and the number of iterations. Table 13 presents the grid values to find the best hyperparameters of the SVR with 5CV using the training dataset. Table A2 shows the configuration of the best strategies found during the simulation, see Appendix A.

The ANN model capacity depends on the number of hidden layers and the neurons per layer. The neural architecture search process empirically looks for the best hyperparameters of the ANN. This procedure is expensive in terms of time and computational resources because every combination of hyperparameters must be evaluated.

Table 14 shows the grid values to find the best hyperparameters of ANN with 5CV using the training dataset and fully connected layers. Table A3 shows the configuration of the best strategies found during the simulation, see Appendix A.

5. Results and discussion

In the present work to correlate the relationship between input and output using different ML models, two approaches were utilized, in the first approach, the number of 20 data sets were taken into account for each material and the metrics were calculated. The second approach used the workpiece material as an input that is quantified by defining the Palatnik index described earlier. The obtained results showed that

Table 11
Number of the instances in the training datasets after the preprocessing stage.

Inputs	Material	N	*MRR*	*EW*	*v*	R_z	R_{sk}
Ψ, t, U, I, p	In + Ti	50	32	34	35	35	33

Table 12
Parameters of RF to find the best prediction model using 5CV.

Parameter	Values
n_estimators	{50, 100, 150, 200, 250, 300}
max_depth	{2, 3, 4, 5, 6, 7}
min_samples_split	{2, 3, 4, 5}
bootstrap	{True, False}

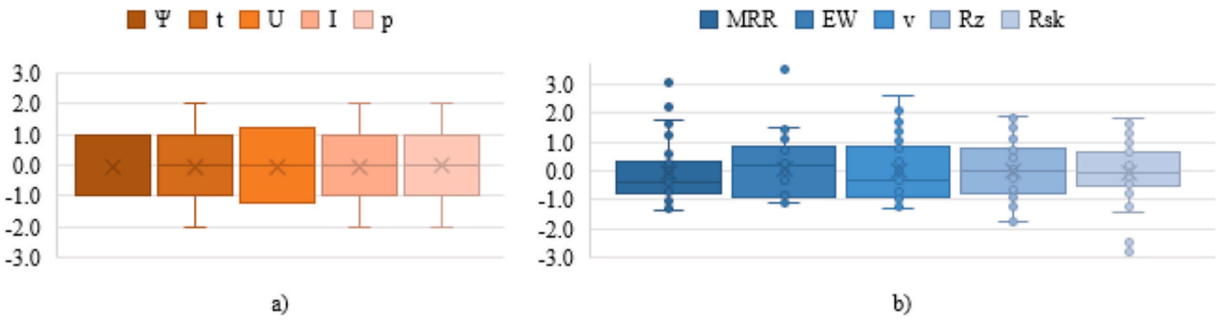

Fig. 12. Standardized a) inputs and b) outputs of the datasets.

Table 13
Parameters of SVR to find the best prediction model using 5CV.

Parameter	Values
Kernel	{ linear, polynomial, radial, sigmoid}
Degree	{2, 3, 4, 5, 6, 7}
Epsilon	{0.1, 0.2, 0.3, 0.4, 0.5}
Iterations	{50, 100, 150, 200}

Table 14
Parameters of ANN to find the best prediction model using 5CV.

Parameter	Values	Total
Epochs	100, 150, 200, 250, 300, 350, 400, 450, 500, 550, 600	11
1 hidden layer (1HL)	10, 20, 30, 40, 50, 60, 70, 80, 90, 100, 110, 120	12
2 hidden layers (1HL-2HL)	10-5, 20-10, 30-15, 40-20, 50-25, 60-30, 70-35, 80-40, 90-45, 100-50, 110-55, 120-60	12
3 hidden layers (1HL-2HL-3HL)	5-10-5, 10-20-10, 15-30-15, 20-40-20, 25-50-25, 30-60-30, 35-70-35, 40-80-40, 45-90-45, 50-100-50, 55-110-55, 60-120-60	12
4 hidden layers (1HL-2HL-3HL-4HL)	5-10-10-5, 10-20-20-10, 15-30-30-15, 20-40-40-20, 25-50-50-25, 30-60-60-30, 35-70-70-35, 40-80-80-40, 45-90-90-45, 50-100-100-50, 55-110-110-55, 60-120-120-60	12
Activation function	Hyperbolic tangent (tanh), Logistic, Rectified Linear Unit (ReLU)	3
Learning rate	0.05, 0.01, 0.005, 0.001	4

the prediction accuracy in second approach is much better due to contribution of more data in developing the ML models. However, as the difference was significant, here in order to avoid confusion by bringing the tables and figures, the results of first approach was left behind and only the second approach as the main modeling strategy is described.

The comparison of performance of different ML models i.e. LR, SVR, RF and ANN in prediction of MRR, EW, v, R_z and R_{sk} based on the different metrics i.e. MSE, RMSE, R^2 and MAPE for the testing data have been presented in Fig. 13. According to the figure, it is seen that for all the metrics, the ANN outperforms other ML models in prediction of the data sets which were not included in the training in correlation of process factors to MRR, v, R_z and R_{sk}. However, it is seen that only in case pf prediction of EW, the RF is slightly better than ANN while still the ANN is by far outperforms LR and SVR. In other words, in prediction of MRR, v, R_{sk} and R_z, taking into accounts the metrics MSE, RMSE and MAPE, the ANN has the lowest value, and for the metric R^2 it adopts the maximum value confirming the better accuracy of this ML model compared to others. On the other hand, in the case of EW, it is seen that the RF for the metrics MSE, RMSE, MAPE has the lowest value, while for R^2 it has the highest amount. It is seen that the prediction errors for R_z and R_{sk} are rather higher than other outputs that can be referred to the chaotic nature of roughness distribution in EDM process that was reported in Sections 3.3 and Section 3.4.

Fig. 14a–e represent the comparison between actual and predicted values of testing data based on SVR, ANN, LR, and RF models trained with both datasets (Inconel 625 and Titanium Grade 2). In the figure, the first 5 data sets belong to machining of Inconel while the other remaining 4 data is dedicated to machining of Titanium. From the Fig. 14a, it is seen that the among the different types of ML models, the MRR values which were predicted by ANN are very close to actual values where it is in line with the results of different metrics reported in Fig. 13. On the other hand, it is observed from Fig. 14b that the RF has the best accuracy in the case of prediction of electrode wear where the RF predicted values of EW are more compatible with the actual values compared to other networks. Furthermore, on the basis of the Fig. 14c, it is evidence that the ANN outperforms other models in prediction of

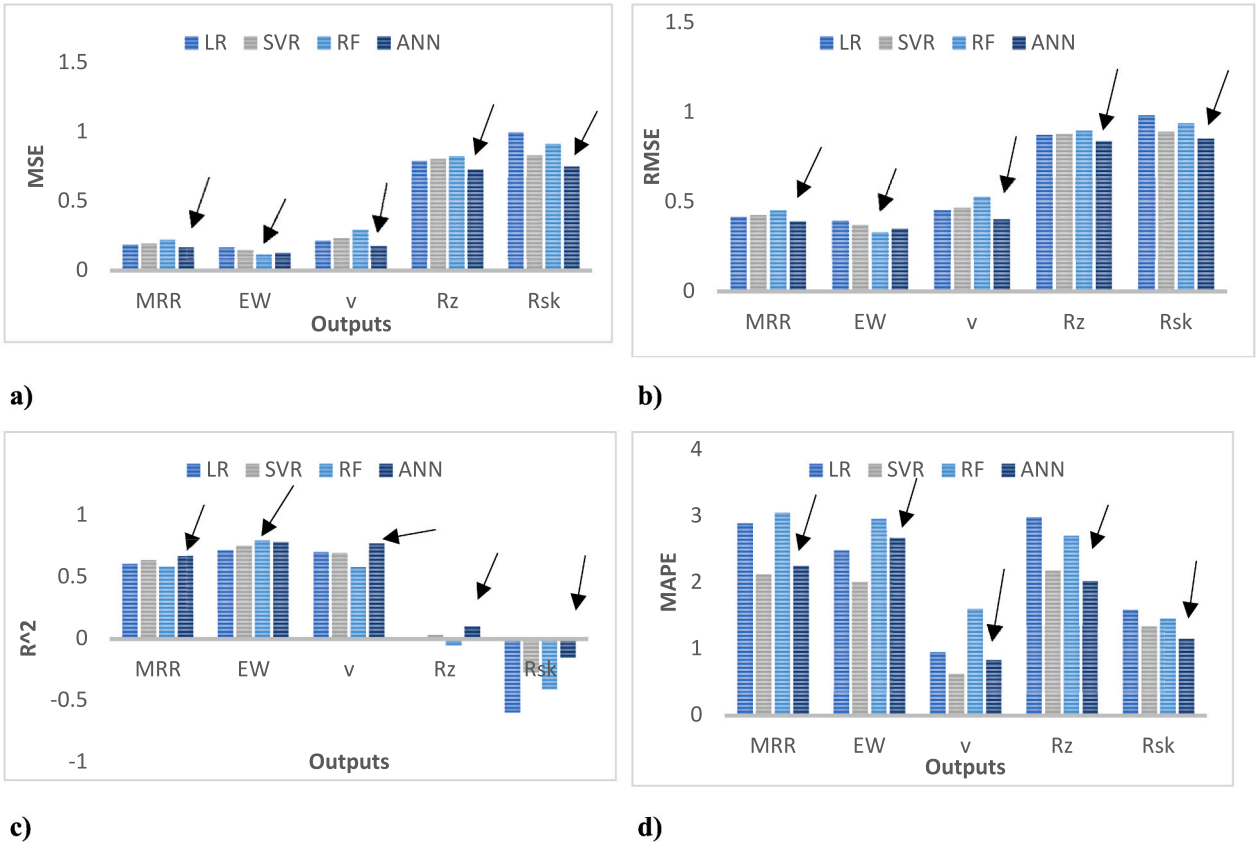

Fig. 13. Comparison of the performance of different ML models in prediction of outputs taking into account different metrics (a) MSE (b) RMSE (c) R^2 and (d) MAPE.

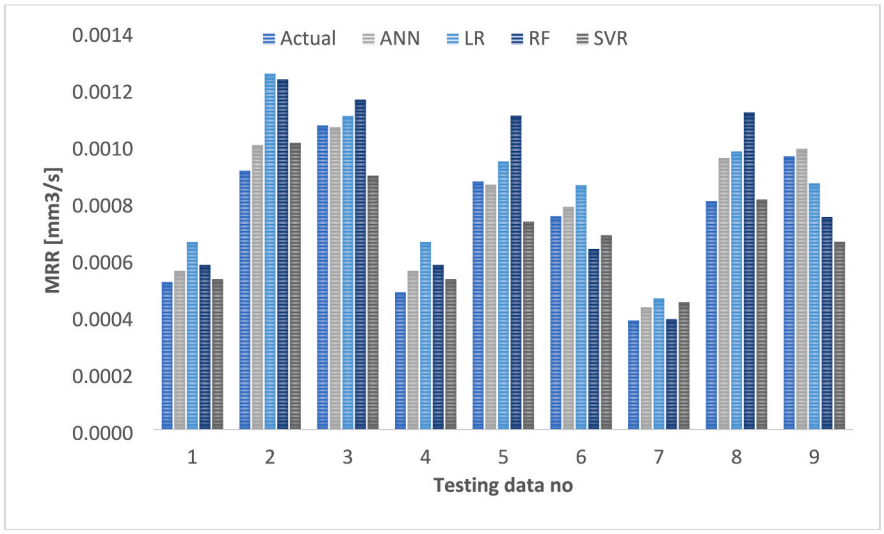

a)

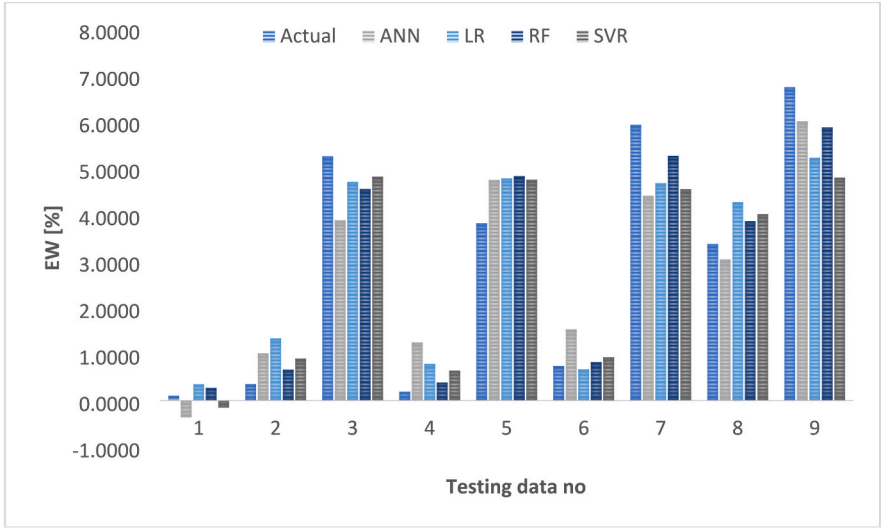

b)

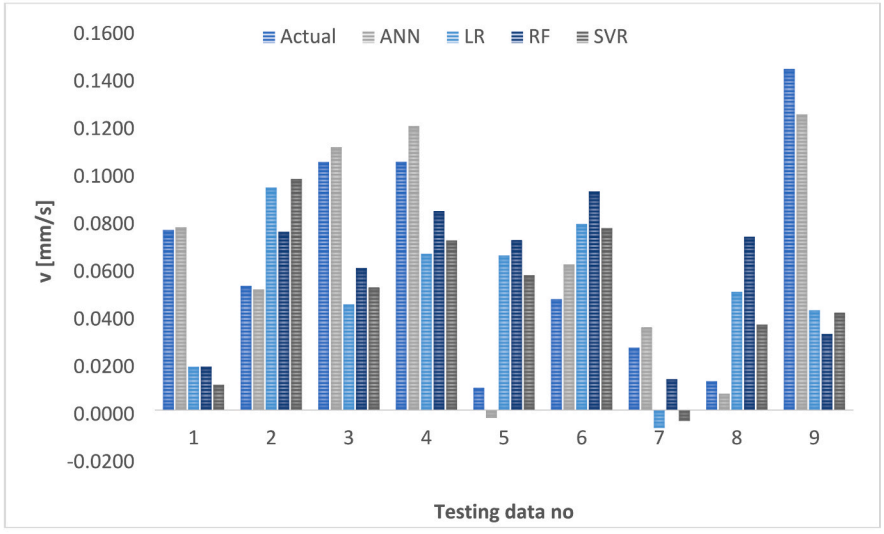

c)

Fig. 14. Comparison of actual and predicted values of outputs obtained from different ML models for testing data (a) MRR (b) EW (c) v (d) R_z (e) $R_{sk.}$

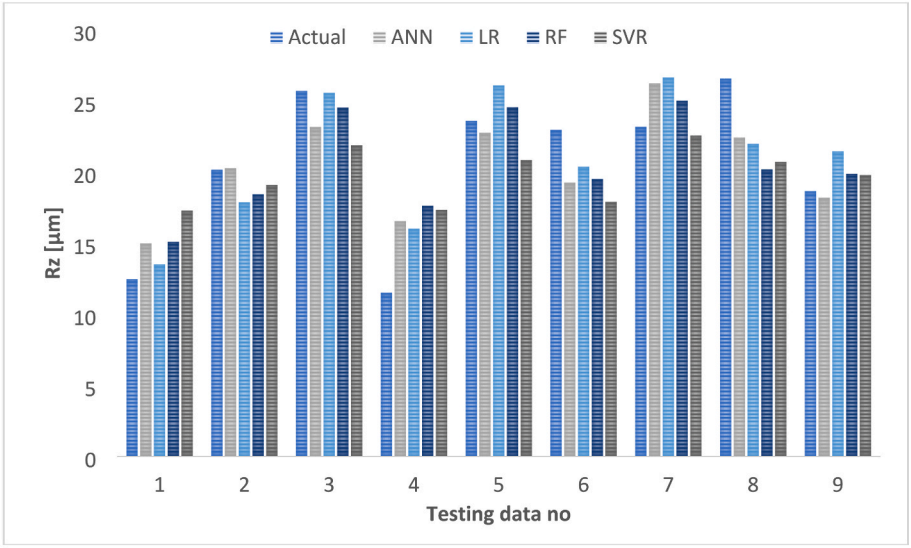

d)

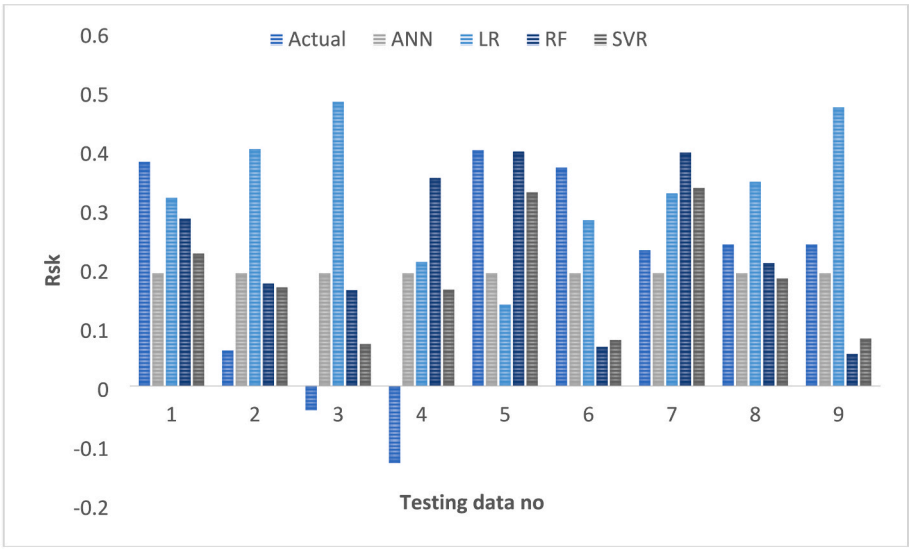

e)

Fig. 14. (*continued*).

working electrode velocity where the other networks don't provide the acceptable prediction. In Fig. 14d, it is seen that the ANN offers best prediction accuracy in prediction of R_z followed by LR, RF and SVR. Finally, in the case of the prediction of R_{sk}, it is observed that the ANN has the better prediction performance compared to other networks, however, as described in the section 3.4, because of uncertainty of the measurement of R_{sk} in the EDM process, the mismatch between the measured and predicted values are higher than other outputs. The root mean square roughness R_z is the average value of the absolute values of the heights of the five highest-profile peaks and the depths of the five deepest alleys within the evaluation length [50]. The hybrid parameter skewness R_{sk} is sensitive to occasional high peaks or deep valleys. A R_{sk} value of 0 would be expected for a surface with symmetrical height distribution (as many peaks as valleys), where profiles filled valleys present R_{sk} below zero [51]. Considering the random nature of the discharge phenomenon during EDM, it is evident that precise control of the various processes occurring within the discharge gas is unfeasible. These processes include, but are not limited to, temperature fluctuations, dielectric breakdown, the removal of machining products, the deposition of workpiece material on the working electrode, and the melting of the working electrode and subsequent deposition on the surface of the workpiece. All of this has a great influence on the structure, depth, and structure of valleys (craters), as well as solidifies flashes after the machining process.

Tables A4 and A5 show the best solutions for the LR and SVR prediction models and Figs. A1 to A5 present some examples of DTs from the RFs solutions, see Appendix A.

6. Conclusion

In the present study, data-driven modeling of a new modification of dry EDM process in presence of coolant has been performed. Here, different ML models, namely, Linear Regression, Support Vector Regression, Artificial Neural Network and Random Forest were utilized to correlate dry EDM outputs i.e. workpiece material, current density, voltage, pulse time and gas pressure, to main process' outputs namely material removal rate, electrode wear, velocity, and surface roughness. The obtained results can be summarized as follows:

- The prediction model with information from both materials improves on average the efficiency of the predictions over all the evaluated models,

- While comparing different metrics for prediction accuracies, it was found that the ANN has the best performance in modeling of MRR, v, R_z and R_{sk}. While the RF is the best in case of EW.
- Compared to other process outputs, the prediction errors for R_{sk} and R_z in all the ML models are found higher that can be attributed to the physics of EDM process that generates the roughness in a very chaotic nature.
- On the basis of obtained results, it was found that the ANN in majority of outputs i.e. MRR, v, R_z and R_{sk} gives the best prediction accuracy for the testing data which were not included in the training. Also, in the case of EW, nevertheless the performance of RF is the best, but it doesn't have significant difference to ANN. Thus, it can be concluded that the ANN can be used as the best ML predictor to correlate the mapping relationship between the process' inputs and outputs to navigate the design space.

In further study, it is needed to introduce the following improvements:

- Development of rotary tool EDM process and analysing the impact of different types of gases on the output of EDM process.
- Use data augmentation and feature engineering strategies to enhance the prediction of output parameters in the machining process.

CRediT authorship contribution statement

Jorge M. Cortés-Mendoza: Writing – original draft, Resources, Methodology, Investigation, Formal analysis, Conceptualization. **Agnieszka Żyra:** Writing – original draft, Resources, Methodology, Investigation, Funding acquisition, Formal analysis, Conceptualization. **Horacio González-Vélez:** Writing – review & editing, Supervision, Methodology, Funding acquisition, Conceptualization.

Declaration of competing interest

The authors declare that they have no known competing financial interests or personal relationships that could have appeared to influence the work reported in this paper.

Acknowledgments

This research was funded by the Irish Research Council under grant GOIPD/2023/1341, "CA19135 - Connecting Education and Research Communities for an Innovative Resource Aware Society (CERCIRAS)," under STSM no. E-COST-GRANT-CA19135-b1b0fe9d; and "DIGITAL4-Security: European Masters Programme in Cybersecurity Management & Data Sovereignty" project (EU Digital Europe Programme grant number 101123430). This research was funded in part by National Science Centre, Poland, under grant number: 2023/07/X/ST8/01186.

Appendix

Table A1
LR, RF, SVR, and ANN prediction performance with Inconel 625 and Titanium datasets, 5CV, and 30 executions, the best values for the four approaches are bolded.

Output	Phase	LR			SVR			RF			ANN		
		MSE	***RMSE***	R^2	***MSE***	***RMSE***	R^2	***MSE***	***RMSE***	R^2	***MSE***	***RMSE***	R^2
MRR	Training	0.1177	0.3419	0.8053	0.1407	0.3726	0.7672	0.0613	0.2452	0.8987	**0.0224**	**0.1389**	**0.9636**
	Testing	0.1868	0.4170	0.6066	0.1945	0.4256	0.6376	0.2215	0.4506	0.5839	**0.1671**	**0.3897**	**0.6735**
EW	Training	0.1213	0.3478	0.8352	0.1381	0.3709	0.8122	0.0473	0.2167	0.9356	**0.0257**	**0.1576**	**0.9651**
	Testing	0.1626	0.3959	0.7180	0.1481	0.3712	0.7525	**0.1143**	**0.3292**	**0.7955**	0.1274	0.3499	0.7851
v	Training	0.1683	0.4094	0.8329	0.1884	0.4330	0.8133	**0.0754**	**0.2715**	**0.9256**	0.1384	0.3704	0.8630
	Testing	0.2139	0.4517	0.7059	0.2295	0.4653	0.6947	0.2924	0.5275	0.5812	**0.1722**	**0.4006**	**0.7739**
R_z	Training	0.5250	0.7230	0.4706	0.3139	0.5573	0.6841	0.4879	0.6976	0.5072	**0.2865**	**0.5336**	**0.7120**
	Testing	0.7897	0.8725	−0.0102	0.8035	0.8777	0.0310	0.8240	0.8957	−0.0503	**0.7275**	**0.8375**	**0.1006**
R_{sk}	Training	0.6200	0.7856	0.0820	**0.3298**	**0.5710**	**0.5130**	0.5069	0.7097	0.2504	0.6830	0.8252	−0.0132
	Testing	0.9952	0.9810	−0.5939	0.8293	0.8910	−0.2685	0.9121	0.9361	−0.4055	**0.7489**	**0.8507**	**−0.1507**

Table A2
Configuration of the best strategies for RF and all the datasets.

Dataset	Parameter	Configuration			
		n_estimators	**max_depth**	**min_samples_split**	**Bootstrap**
Inconel + Titanium	*MRR*	150	6	2	True/False
	EW	100	4	4	True/False
	v	250	6	2	True/False
	R_z	100	2	5	True/False
	R_{sk}	200	2	5	True/False

Table A3
Configuration of the best strategies for SVR and all the datasets.

Dataset	Parameter	Configuration			
		iterations	Epsilon	Kernel	Degree
Inconel + Titanium	*MRR*	100	0.02	Linear	2
	EW	200	0.02	Linear	2
	v	200	0.02	Linear	2
	R_z	50	0.02	Radial	–
	R_{sk}	50	0.02	Radial	–

Table A4
Configuration of the best strategies for ANN and all the datasets.

Dataset	Prediction	Configuration			
		Epochs	Neurons per hidden layers	Activation function	Learning rate
Inconel + Titanium	*MRR*	500	55–110-110–55	ReLU	0.05
	EW	150	80–40	ReLU	0.05
	v	550	30–15	Logistic	0.05
	R_z	100	80	ReLU	0.05
	R_{sk}	200	5–10-10–5	Logistic	0.05

Table A5
Table of coefficients for the best model of LR with normalized values.

	$\widehat{\beta}_0$	$\widehat{\beta}_1$	$\widehat{\beta}_2$	$\widehat{\beta}_3$	$\widehat{\beta}_4$	$\widehat{\beta}_5$
MRR	−0.13441143	−0.062055	0.077938	0.105832	0.617859	0.179875
EW	−0.08057508	−0.706865	0.109636	0.133243	−0.075969	−0.078176
v	−0.02199991	−0.647117	0.104774	0.154047	0.548398	0.162842
R_z	0.05469054	−0.399168	−0.091395	0.135280	0.501958	0.058769
R_{sk}	0.09476015	0.040164	0.093982	0.057728	−0.117807	0.106405

Table A6
Table of coefficients for the best model of SVR with normalized values (only for linear models)*.

	$\widehat{\beta}_0$	$\widehat{\beta}_1$	$\widehat{\beta}_2$	$\widehat{\beta}_3$	$\widehat{\beta}_4$	$\widehat{\beta}_5$
MRR	−0.18234569	−0.02744863	0.05777316	0.13236128	0.59507204	0.11561341
EW	−0.11461549	−0.73449764	0.07288629	0.12871271	−0.07281424	−0.02757991
v	−0.04829821	−0.63512199	0.14443802	0.14994380	0.52027816	0.17861080

*The best models for R_z and R_{sk} use radial kernels that consist of matrices, so they are not defined in this table.

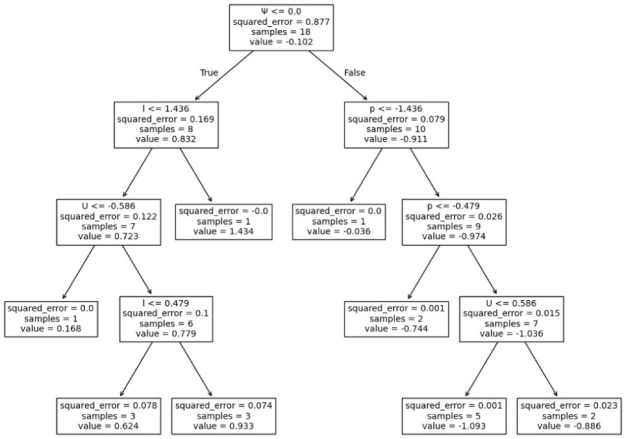

Fig. 2A. An example of a DT from the RF regressor for the prediction of with normalized values

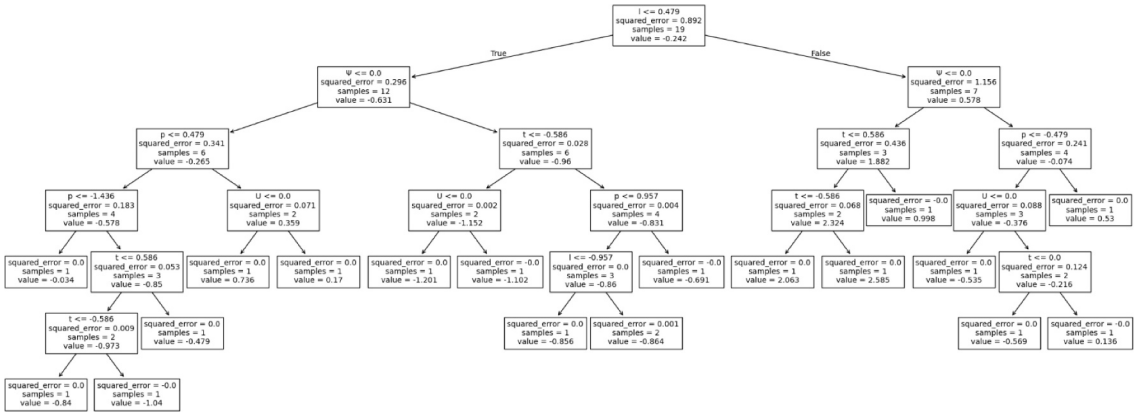

Fig. 3A. An example of a DT from the RF regressor for the prediction of with normalized values

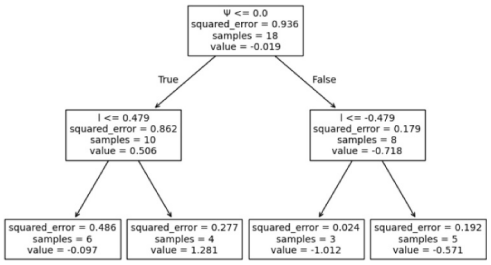

Fig. 4A. An example of a DT from the RF regressor for the prediction of with normalized values

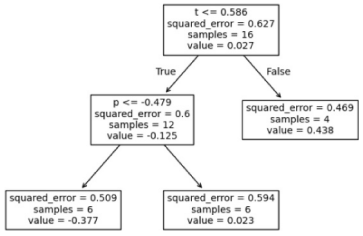

Fig. 5A. An example of a DT from the RF regressor for the prediction of with normalized values

Data availability

Data will be made available on request.

References

[1] E. Şentürk, C. Alparslan, Ş. Bayraktar, M.E. Korkmaz, M. Günay, A comprehensive review on sustainability in EDM process of additive manufactured materials, *Measurement* 245 (Mar. 2025) 116626, https://doi.org/10.1016/J.MEASUREMENT.2024.116626.

[2] P. Govindan, A. Gupta, S.S. Joshi, A. Malshe, K.P. Rajurkar, Single-spark analysis of removal phenomenon in magnetic field assisted dry EDM, *J. Mater. Process. Technol.* 213 (7) (2013) 1048–1058, https://doi.org/10.1016/j.jmatprotec.2013.01.016.

[3] R. Teimouri, H. Baseri, Experimental study of rotary magnetic field-assisted dry EDM with ultrasonic vibration of workpiece, *Int. J. Adv. Manuf. Technol.* 67 (5–8) (2013) 1371–1384, https://doi.org/10.1007/s00170-012-4573-6.

[4] S. Joshi, P. Govindan, A. Malshe, K. Rajurkar, Experimental characterization of dry EDM performed in a pulsating magnetic field, *CIRP Ann. - Manuf. Technol.* 60 (1) (2011) 239–242, https://doi.org/10.1016/j.cirp.2011.03.114.

[5] S.T. Kumaran, T.J. Ko, R. Kurniawan, Grey fuzzy optimization of ultrasonic-assisted EDM process parameters for deburring CFRP composites, *Measurement* 123 (2018) 203–212, https://doi.org/10.1016/J.MEASUREMENT.2018.03.076.

[6] G. Skrabalak, J. Kozak, M. Zybura, Optimization of dry EDM milling process, *Procedia CIRP* 6 (2013) 332–337, https://doi.org/10.1016/j.procir.2013.03.027.

[7] Y. Shen, Y. Liu, W. Sun, High-efficient Dry Hybrid Machining of EDM and Arc Machining, *Procedia CIRP* 42 (2016) 149–154, https://doi.org/10.1016/j.procir.2016.02.210.

[8] N.K. Singh, P.M. Pandey, K.K. Singh, M.K. Sharma, Steps towards green manufacturing through EDM process: a review, Cogent. Eng. 3 (1) (2016), https://doi.org/10.1080/23311916.2016.1272662.

[9] Y. Shen, et al., High-speed near dry electrical discharge machining, *J. Mater. Process. Technol.* 233 (Jul. 2016) 9–18, https://doi.org/10.1016/J.JMATPROTEC.2016.02.008.

[10] S. Boopathi, A.S. Alqahtani, A. Mubarakali, P. Panchatcharam, Sustainable developments in near-dry electrical discharge machining process using sunflower oil-mist dielectric fluid, Environ. Sci. Pollut. Res. 0123456789 (2023), https://doi.org/10.1007/s11356-023-27494-0.

[11] J. Tao, A.J. Shih, J. Ni, Near-dry EDM milling of mirror-like surface finish, Int. J. Electr. Mach. 13 (13) (2008) 29–33.

[12] C.C. Kao, J. Tao, A.J. Shih, Near dry electrical discharge machining, *Int. J. Mach. Tools Manuf.* 47 (15) (2007) 2273–2281, https://doi.org/10.1016/j.ijmachtools.2007.06.001.

[13] X. Bai, Q. Zhang, J. Zhang, D. Kong, T. Yang, Machining efficiency of powder mixed near dry electrical discharge machining based on different material combinations of tool electrode and workpiece electrode, *J. Manuf. Process.* 15 (4) (2013) 474–482, https://doi.org/10.1016/j.jmapro.2013.09.005.

[14] P.R. Cheke, S. Khedekar, P.R.S. Pawar, M.S. Kadam, Comparative performance of wet and near-dry EDM process for machining of oil hardned non sinking steel material, *Int. J. Mech. Eng. Technol.* 0976 (2) (2012) 976–6359.

[15] W. Rajhi, S. Ezeddini, S. Alshammrei, M. Boujelbene, On the identification of the performance characteristics laws in EDM of biomedical Ti-6Al-4V alloy with

different tool electrode materials, *Measurement* 231 (2024) 114656, https://doi.org/10.1016/J.MEASUREMENT.2024.114656.
[16] K. Dhakar, A. Dvivedi, Experimental investigation on near-dry EDM using glycerin-air mixture as dielectric medium, *Mater. Today Proc.* 4 (4) (2017) 5344–5350, https://doi.org/10.1016/J.MATPR.2017.05.045.
[17] B.P. Mishra, B.C. Routara, Evaluation of technical feasibility and environmental impact of Calophyllum Inophyllum (Polanga) oil based bio-dielectric fluid for green EDM, *Meas. J. Int. Meas. Confed.* 159 (2020), https://doi.org/10.1016/j.measurement.2020.107744.
[18] J. Tao, A.J. Shih, J. Ni, Experimental study of the dry and near-dry electrical discharge milling processes, *J. Manuf. Sci. Eng. Trans. ASME* 130 (1) (2008) 0110021–0110029, https://doi.org/10.1115/1.2784276.
[19] M. Kiran, S. Joshi, Modeling of surface roughness and the role of debris in micro-EDM, *J. Manuf. Sci. Eng. ASME* 129 (2007) Apr, https://doi.org/10.1115/1.2540683.
[20] Q.H. Zhang, R. Du, J.H. Zhang, Q.B. Zhang, An investigation of ultrasonic-assisted electrical dischargemachining in gas, *Int. J. Mach. Tools Manuf.* 46 (12–13) (2006) 1582–1588.
[21] P.C. Tan, S.H. Yeo, Modelling of overlapping craters in micro-electrical discharge machining, *J. Phys. D. Appl. Phys.* 41 (20) (2008) 205302, https://doi.org/10.1088/0022-3727/41/20/205302.
[22] W. Kurnia, P.C. Tan, S.H. Yeo, Q.P. Tan, Surface roughness model for micro electrical discharge machining, Proc. Inst. Mech. Eng. Part B J. Eng. Manuf. 223 (3) (2009) 279–287, https://doi.org/10.1243/09544054JEM1188.
[23] B. Izquierdo, J.A. Sánchez, S. Plaza, I. Pombo, N. Ortega, A numerical model of the EDM process considering the effect of multiple discharges, *Int. J. Mach. Tools Manuf.* 49 (3–4) (2009) 220–229, https://doi.org/10.1016/j.ijmachtools.2008.11.003.
[24] J.F. Liu, Y.B. Guo, Thermal modeling of EDM with progression of massive random electrical discharges, *Procedia Manuf.* 5 (2016) 495–507, https://doi.org/10.1016/j.promfg.2016.08.041.
[25] S. Jithin, A. Raut, U.V. Bhandarkar, S.S. Joshi, Finite element model for topography prediction of electrical discharge textured surfaces considering multi-discharge phenomenon, *Int. J. Mech. Sci.* 177 (2020) 105604, https://doi.org/10.1016/j.ijmecsci.2020.105604.
[26] Y. Anagün, Ş. Işik, F. Hayati Çakir, Surface roughness classification of electro discharge machined surfaces with deep ensemble learning, Measurement 215 (2023) 112855, https://doi.org/10.1016/J.MEASUREMENT.2023.112855.
[27] M.A. Rahman Khan, M.M. Rahman, K. Kadirgama, Neural network modeling and analysis for surface characteristics in electrical discharge machining, Procedia Eng. 90 (2014) 631–636, https://doi.org/10.1016/J.PROENG.2014.11.783.
[28] A.S. Bhandare, U.A. Dabade, Modeling of dry EDM process parameters during machining of Inconel 718 using artificial neural network, *Mater. Today Proc.* (2023), https://doi.org/10.1016/j.matpr.2023.08.293.
[29] K. Ishfaq, M. Sana, W.M. Ashraf, V. Dua, Sustainable EDM of Inconel 600 in Cu-mixed biodegradable dielectrics: modelling and optimizing the process by artificial neural network for supporting net-zero from industry, *J. Clean. Prod.* 421 (2023) 138388, https://doi.org/10.1016/J.JCLEPRO.2023.138388.
[30] M. Quarto, G. D'Urso, C. Giardini, Micro-EDM optimization through particle swarm algorithm and artificial neural network, *Precis. Eng.* 73 (2022) 63–70, https://doi.org/10.1016/J.PRECISIONENG.2021.08.018.
[31] J. Martin Sahayaraj, R. Arravind, P. Subramanian, S. Marichamy, B. Stalin, Artificial neural network based prediction of responses on eglin steel using electrical discharge machining process, Mater. Today: Proc. 33 (2020) 4417–4419, https://doi.org/10.1016/j.matpr.2020.07.664.
[32] S. Velpula, K. Eswaraiah, S. Chandramouli, Prediction of electric discharge machining process parameters using artificial neural network, 2019.
[33] V.R. Surya, K.M. Vinay Kumar, R. Keshavamurthy, G. Ugrasen, H.V Ravindra, Prediction of machining characteristics using artificial neural network in wire EDM of Al7075 based in-situ composite, 2017.
[34] S. Kumar, S. Kumar, R. Sharma, M. Singh, R. Singh, Artificial neural network based modeling to predict micro-hardness during EDM of cryo-treated titanium alloys, *Mater. Today Proc.* 56 (2022) 2938–2944, https://doi.org/10.1016/j.matpr.2021.10.426.
[35] N. Mondal, S. Nishant, M.C. Ghosh, S.P. Mandal, S. Banik, ANN and RSM based predictive model development and EDM process parameters optimization on AISI 304 stainless steel, *Mater. Today Proc.* (2023), https://doi.org/10.1016/j.matpr.2023.01.322.
[36] S. Ganapathy, P. Balasubramanian, B. Vasanth, S. Thulasiraman, Comparative investigation of Artificial Neural Network (ANN) and Response Surface Methodology (RSM) expectation in EDM parameters, *Mater. Today Proc.* 46 (2019) 9592–9596, https://doi.org/10.1016/j.matpr.2020.05.499.
[37] V. Kanake, B.B. Ahuja, Prediction of tool wear length in micro-EDM process using an artificial neural network, *Mater. Today Proc.* 63 (2022) 107–112, https://doi.org/10.1016/j.matpr.2022.02.345.
[38] A. Cetin, G. Atali, C. Erden, S.S. Ozkan, Assessing the performance of state-of-the-art machine learning algorithms for predicting electro-erosion wear in cryogenic treated electrodes of mold steels, *Adv. Eng. Inform.* 61 (2024) 102468, https://doi.org/10.1016/J.AEI.2024.102468.
[39] A. Żyra, S. Skoczypiec, R. Bogucki, Selected aspects of surface integrity of inconel 625 alloy after dry-EDM in carbon dioxide, *Key Eng. Mater.* 926 (2022) 1681–1688.
[40] A. Żyra, W. Bizoń, S. Skoczypiec, Primary research on dry electrodischarge machining with additional workpiece cooling, AIP Conf. Proc. 2017 (2018), https://doi.org/10.1063/1.5056297.
[41] M. Cotea, L. Santo, T. Gr, Thermal properties of the workpiece material and the machinability by electroerosion, 2009, pp. 219–224.
[42] A. Hrituc, et al., Wear of the tool electrode at simultaneous electrical discharge machining of different materials, *Procedia CIRP* 95 (2020) 419–424, https://doi.org/10.1016/J.PROCIR.2020.02.312.
[43] L. Slatineanu, M. Coteata, O. Dodun, D. Anton, Method for the evaluation of the materials machinability by electrical discharge machining, *Int. J. Mach. Mach. Mater.* 5 (2009), https://doi.org/10.1504/IJMMM.2009.023396.
[44] E. Stępniowska, Wpływ długotrwałego wyżarzania na mikrostrukturę i własności stopu Ni−25Mo−8Cr, *Rozpr. doktorska*.
[45] A. Gupta, T. S. Stead, L. Ganti, Determining a meaningful R-squared value in clinical medicine, 2024, pp. 1–6. https://doi.org/10.62186/001c.125154.
[46] K.P. Murphy, *Probabilistic Machine Learning: Advanced Topics*, MIT Press, 2023.
[47] K.P. Murphy, Probabilistic Machine Learning: Advanced Topics, MIT Press.
[48] O.I. Abiodun, A. Jantan, A.E. Omolara, K.V. Dada, N.A.E. Mohamed, H. Arshad, State-of-the-art in artificial neural network applications: A survey, *Heliyon* 4 (11) (2018) e00938, https://doi.org/10.1016/j.heliyon.2018.e00938.
[49] Y. Chen Wu, J. Wen Feng, Development and application of artificial neural network, *Wirel. Pers. Commun.* 102 (2) (2018) 1645–1656, https://doi.org/10.1007/s11277-017-5224-x.
[50] D. Kumar, M.S. Sisodiya, D.K. Mandal, V. Bajpai, Maglev micro-EDM: feasibility and performance on Inconel 625, *CIRP J. Manuf. Sci. Technol.* 40 (Feb. 2023) 155–166, https://doi.org/10.1016/j.cirpj.2022.11.012.
[51] M. I. Conference, New Production Technologies in Aerospace Industry, no. September, 2014.